UNIVERSITY OF CALIFORNIA SAN DIEGO

What Can Igneous Intrusions Tell Us About Geomagnetic Field Variation?

A Thesis submitted in partial satisfaction of the requirements
for the degree Master of Science

in

Earth Sciences

by

Veronica Yonce

Committee in charge:

Professor Jeffrey Gee, Chair
Professor Catherine Constable
Professor Emily Van Allen (Chin)

2024

©

Veronica Yonce, 2024

All rights reserved.

The Thesis of Veronica Yonce is approved, and it is acceptable in quality and form for publication on microfilm and electronically.

University of California San Diego

2024

TABLE OF CONTENTS

LIST OF FIGURES

LIST OF TABLES

LIST OF ABBREVIATIONS

PSV	Paleosecular Variation
TRM	Thermoremanence Magnetization
PADM	Paleomagnetic Axial Dipole Moment
PADM2M	Paleomagnetic Axial Dipole Moment for the last 2 million years
N	Normal
R	Reverse
MDL	Mesozoic Dipole Low
SD	Single Domain
CJ98	Statistical field model by Constable & Johnson (1999)
GGF100k	Geomagnetic Global Field Model spanning the past 100 kyr
GPTS	Geomagnetic Polarity Time Scale
kyr	Thousand years
myr	Million years

ACKNOWLEDGEMENTS

I would like to acknowledge Professor Jeffrey Gee, Professor Catherine Constable, and Professor Emily Van Allen for being my part of my committee. A special thank you to Professor Jeffrey Gee, the chair of my committee, for taking me on as a master's student and guiding me through the physics-intensive realm of paleomagnetism. I also appreciate the patience you showed while learning how to compile Lesleis Nagy's code and creating the numerical modeling on MATLAB, when neither of us had done that before.

Speaking of Lesleis Nagy, I would like to acknowledge him for taking the time out of his busy schedule to go through the operations of his single domain modeling code. Without his help, and the access he provided to the University of Liverpool's supercomputer, we would have never made any initial progress with our project.

I would also like to thank and acknowledge Peter Selkin for being with me every step of the way. The weekly meetings and time you took to explain new concepts to me definitely did not go unnoticed. I appreciate the patience and kindness you showed to someone new to the field.

Thank you, Nicole Clizzie, for running the GGF100k model we needed for our results. This thesis would not have a proper ending without your help.

Finally, thank you to my friends and family who encouraged me over this past year. Your support is forever appreciated.

ABSTRACT OF THE THESIS

What Can Igneous Intrusions Tell Us About Geomagnetic Field Variation?

by

Veronica Yonce

Master of Science in Earth Sciences

University of California San Diego, 2024

Professor Jeffrey Gee, Chair

Long term variations of the geomagnetic field are one of the few sources of information about the evolution of our planet's deep structure throughout time. Most information about past field variations is derived from studies of lava flows or sedimentary sequences. Slowly-cooled igneous intrusions are rarely used to study geomagnetic field variability because the smoothing of field variations accompanying slow cooling is poorly understood. Many large intrusions have remanence carried by precise, elongate magnetite grains hosted within silicate minerals that

could provide reliable records of directional and intensity fluctuations of the field. Many such intrusions are available throughout geologic time and could provide a new source of information on geomagnetic field variations if the effects of slow cooling can be quantified. Here we use the single domain magnetic code provided by Nagy et al. (2021) to analyze how thermoremanence is acquired in slowly-cooled intrusions over various timescales (lab timescales – hundreds of thousands of years). We find that statistical models of geomagnetic variability, because they are not serially correlated in time, result in magnetizations far smoother than observed in large intrusions. In contrast, a Geomagnetic Global Field model spanning the past 100 kyr, has temporally correlated variations including a short excursion that can be recognized (although smoothed) in the modeled remanence of slowly-cooled intrusions. Earth-realistic field models in conjunction with our model can give a good representation of variability recorded over slow cooling and may potentially allow a geomagnetic signal to be recovered from large intrusions.

Chapter 1 INTRODUCTION

Earth's magnetic field is important to study, as it has long been used as a means for navigation, and serves as a protective barrier by shielding the planet from energetic particle radiation emitted by the Sun. The magnetic field also provides a look into the past, yielding valuable information about how our planet has evolved over geologic time. Turbulent motion of iron in the liquid outer core is what generates the magnetic field. As a result of this constant motion, the magnetic field measured at Earth's surface can vary both in space and time.

When averaged over a sufficiently long-time interval, the structure of the magnetic field is relatively simple, corresponding to a dipolar field aligned with Earth's spin axis. Inclination and declination gathered from geologic materials can be used to estimate past plate motions.

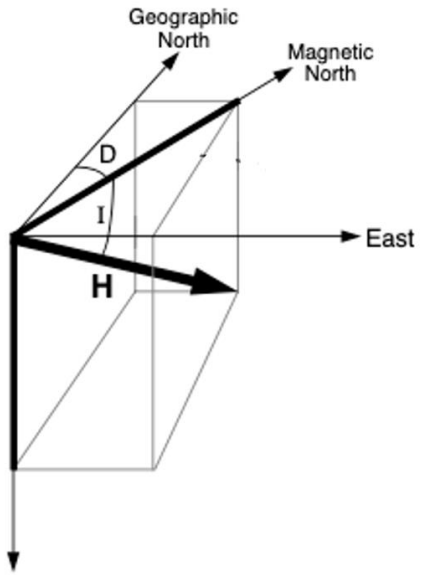

Figure 1.1. Schematic of the magnetic field vector from Butler (2004). Declination, D, is the angle between geographic north and magnetic north along the horizontal plane. Inclination, I, is the angle relative to the horizontal plane.

For such a time-averaged, dipolar field, the inclination (angle of field lines relative to the local horizontal, I in Figure 1.1) varies systematically, from being horizontal at the equator to vertical

at the poles. Geologic materials can preserve a record of the ambient magnetic field when they form. The inclination of the rock's magnetization provides information about the latitude at which it formed, whereas the declination (angle within the horizontal plane relative to true north, D in Figure 1.1) indicates the direction towards the spin axis.

The magnetic field also undergoes polarity reversals, where it flips from a configuration similar to today (called normal polarity) to the opposite state (called reverse polarity). Think of the reverse polarity as a compass whose needle would point toward the south geomagnetic pole. The pattern of these normal and reverse polarity intervals over the past ~160 million years is well established from sea surface magnetic anomaly data, showing how the seafloor can preserve a record of reversals as it cools and drifts away from the mid-ocean ridge (Gee & Kent, 2007). The length of these polarity intervals varies widely, from long intervals of uniform polarity (e.g. Cretaceous Long Normal, 121-83 Ma) to polarity intervals as short as a few tens of thousands of years (Cande and Kent, 1995). The pattern, being sufficiently distinctive, can often be used as a chronological tool; The barcode-like pattern of normal and reverse polarity recorded, for example, in a sequence of sediments can be matched to the established pattern known from the seafloor.

Long term variations of the geomagnetic field are one of the only sources available to get information about the evolution of our planet's deep structure throughout its lifetime. For example, long (40-60 myr) intervals of uniform polarity in the Cretaceous and late Paleozoic have been linked to increased heat flux across the core/mantle boundary resulting from cold subducted slabs or the initiation of plumes (e.g. Larson and Olson, 1991, Biggin et al, 2012). Although most studies linking the geomagnetic field and large-scale geodynamic processes have focused on how frequently the field reverses, fluctuations in geomagnetic intensity or variability

in field directions can also provide information that complements the reversal record. Many recent studies (e.g. Bono et al., 2019) have suggested a possible link between extremely weak intensities near the beginning of the Paleozoic and the nucleation of the solid inner core. A possible correlation between long intervals of constant polarity and a stronger, more directionally stable field has also been suggested (e.g. Tauxe and Staudigel, 2004).

Although directional and intensity variations of the geomagnetic field can provide valuable information over a wide range of time scales, here we are focused on field variations over 100s of years to 100,000s of years, commonly referred to as paleosecular variation (PSV). The full range of the time-varying geomagnetic field is illustrated in the power spectrum shown in Figure 1.2 (Constable and Constable, 2023).

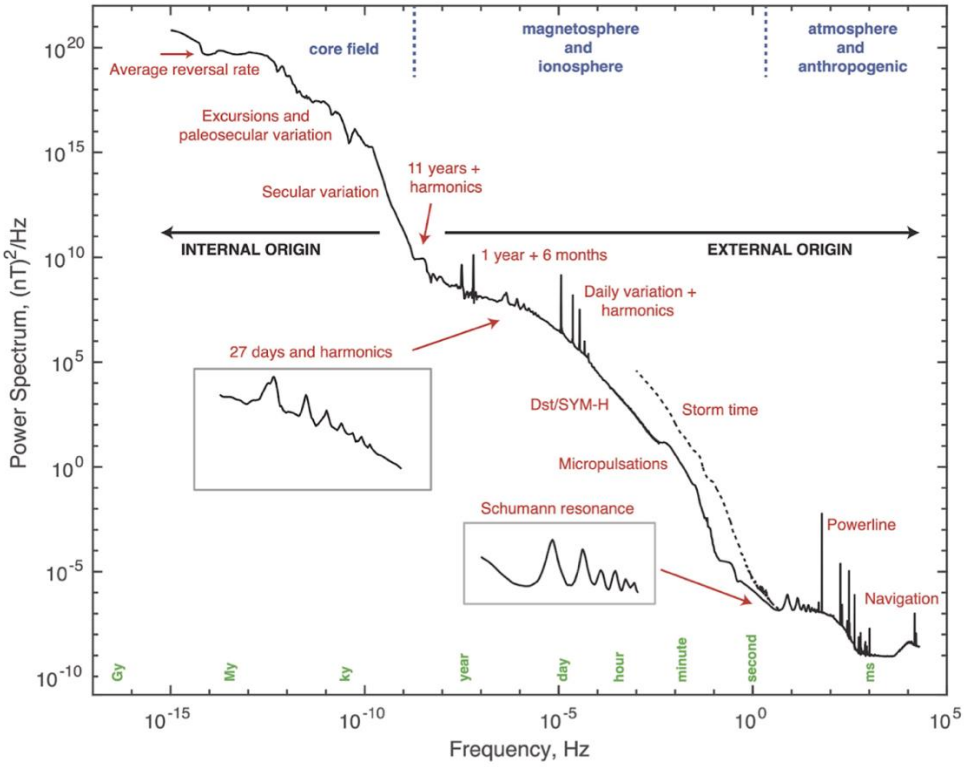

Figure 1.2. The Grand Spectrum of the geomagnetic field as produced by Constable & Constable (2023).

On the longest time scales, variations are dominated by polarity reversals (e.g. Cande and Kent, 1995; GPTS 2012 from Gradstein et al., 2012). On time scales shorter than about 10 years, field variations are dominantly external in origin (Constable & Constable, 2023), meaning they result from interactions between Earth's external magnetic field and contributions such as solar wind, lightning, power systems, and radio transmissions. PSV studies focus on relatively short time variations that are of internal origin but may extend to time scales of a few hundred thousand years (the average reversal rate of about 4 per million years in the Cenozoic, Lowrie and Kent, 2004) beyond which geomagnetic variations are dominated by polarity reversals.

In this study, we look at whether large, layered mafic intrusions can potentially provide information on intermediate to long time variation – timescales associated with PSV – of the geomagnetic field (ky – My timescale as shown by the Grand Spectrum in Figure 1.2). Information about geomagnetic variation on these timescales can be obtained from continuous sedimentary records, but many of these studies have concentrated on younger sediments, which don't tell us much about variations on longer timescales. Slowly-cooled igneous intrusions are rarely used to study geomagnetic field variability because the smoothing accompanying slow cooling is poorly understood. Slowly-cooled mafic intrusions that have silicate-hosted magnetite, which are single domain-like grains and will be discussed further below, turn out to be great recorders of the field. This study will address the smoothing imparted during slow cooling, a necessary first step in evaluating whether large intrusions may yield records of geomagnetic field variations.

1.1 - What is PSV and how is it studied?

Ideally, PSV could be constrained from time series of geomagnetic variations, including both directional and intensity fluctuations, from many sites around the globe. In practice, though, much more limited paleomagnetic data is available, as we are restricted to areas of rock that are exposed at the surface today (Johnson & McFadden, 2007), and hope they have the desired range of ages we want to study. Historical observations of geomagnetic variations extend only over the past few hundred years (e.g. Bloxham et al., 1989). Archeological materials, such as pottery or kilns, that have been heated and then cooled in the field can provide estimates of geomagnetic intensity and direction that extend back a few thousand years. Over longer time scales we must turn to geological materials such as lava flows and sedimentary sequences. Most PSV studies have used rapidly cooled lava flows (e.g., Love, 2000), as these flows can capture a snapshot of what the geomagnetic field was like when the flow cooled, and can provide full information on declination, inclination and, in principle, an estimate of absolute intensity. For some samples, the initial thermoremanence (TRM) acquired during cooling can be replicated by cooling in a known field in the lab. This can give a good estimate of absolute intensity (Tauxe & Yamazaki, 2015) but typically only a small percentage of samples yield reliable data. In addition, these data from lava flows are sporadic in nature, as both locations and frequency of eruptions can vary greatly. Because of these limitations, PSV studies of lavas often focus on statistical descriptions (see below) of the directional variability of the field.

The irregular timing of lava flows makes it difficult to construct a time series from this type of data. A statistical approach can be much more useful in these scenarios. By taking multiple samples from a single lava flow one can determine how much directional variation there

is due to laboratory and sampling uncertainty. The remaining directional scatter between lava flows should then give useful information about the variability of the field. The Fisher distribution is commonly used to describe the statistics of spherical data and is useful when wanting to characterize the directional variation of lava data. The Fisher probability distribution function, Equation 1 (Butler, 2004), is represented in terms of κ, the measure of the how tight the distribution is about the true mean direction, and has θ as the angle from true mean ($\theta = 0$ at the true mean).

$$\text{Equation 1: } P_{dA}(\theta) = \frac{\kappa}{4\pi \sinh(\kappa)} \exp(\kappa \cos\theta)$$

Kappa is the property of the underlying Fisher distribution which we can only estimate from any finite sample from the distribution. The best estimate of kappa (denoted by k) is related to the amount of directional scatter in the distribution. It is a measure of the dispersion relative to the mean and is related to variance in these directions. Directions from geologic materials can give insights on the amount of variation within the field at time of cooling; $k = 0$ when the directions are uniform over a sphere and increases in magnitude as the concentration of the distribution of directions is closer to the true mean direction (Butler, 2004). As Figure 1.3 demonstrates, a larger κ value will give more tightly clustered directional variation ($k = 50$ for some of the bottom plots), and a smaller value will give more dispersion ($k = 5$ for the top plots).

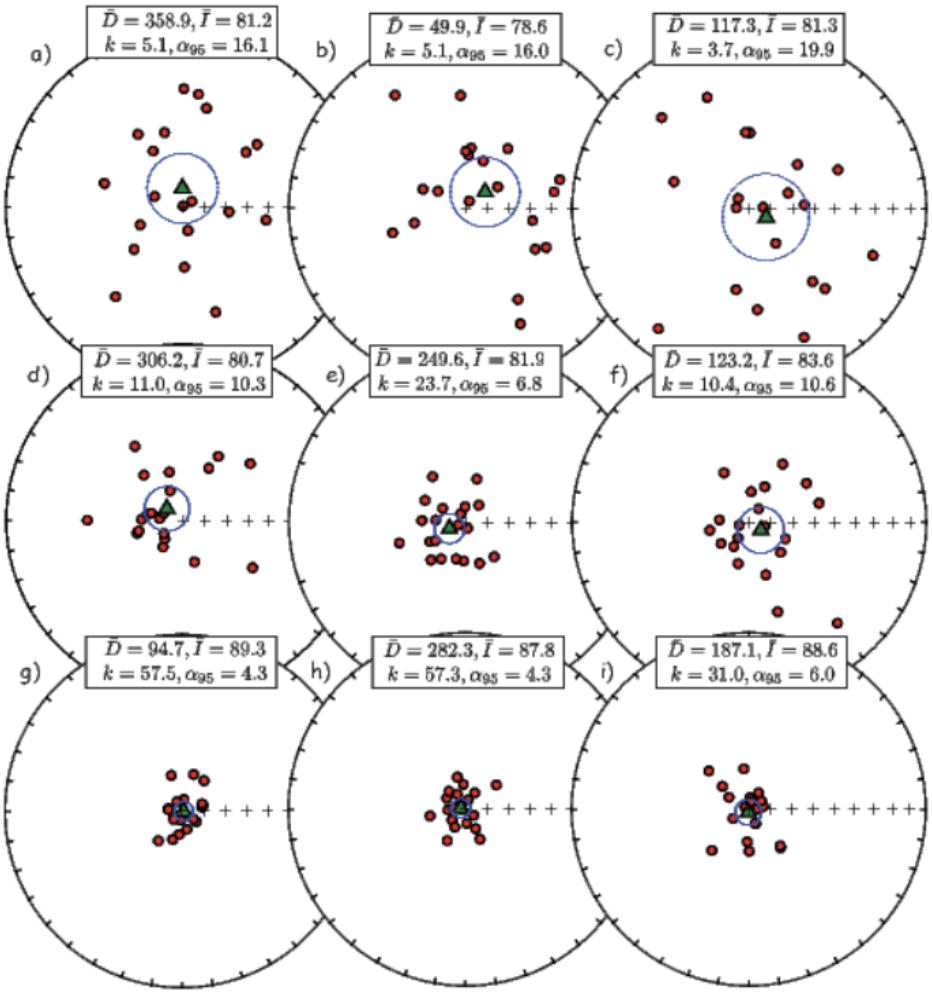

Figure 1.3. Example data sets from Tauxe et al. (2018) that uses Fisher distributions with varying k values. Lower k values give more scatter, and a higher k will have more tightly clustered data. $\alpha 95$ is a measure of the uncertainty of the mean and therefore is dependent on the number of samples used to estimate the mean.

Sediment cores can provide near continuous records of field variability with potentially broad spatial coverage. Sediment cores are typically not azimuthally oriented, so only declination changes (and not absolute declination values) can be determined. Despite this limitation, variations in inclination from sediment cores have provided valuable information on deviations of the field from a pure geocentric axial dipole (e.g. Schneider and Kent, 1990). In contrast to the thermoremanence magnetization (TRM) in lava flows, there is no theoretical basis for relating the magnitude of sedimentary magnetization to the ambient field intensity during deposition (e.g.

Tauxe & Yamazaki, 2015). Estimates of the relative intensity of the geomagnetic field can be made by normalizing the measured magnetization by some proxy for how much magnetic material is present. As a result, many studies have focused on relative intensity derived from cores, and a significant number of records are now available with many having independent chronologies from oxygen isotopic variations in the same cores.

Relative intensity records from sediments can be combined with absolute intensity estimates to yield an estimate of how the most significant component of Earth's magnetic field, the axial dipole, has varied in the past. Figure 1.4 shows an estimate of the paleomagnetic axial dipole moment (PADM) spanning the past two million years (PADM2M, Ziegler et al., 2011)

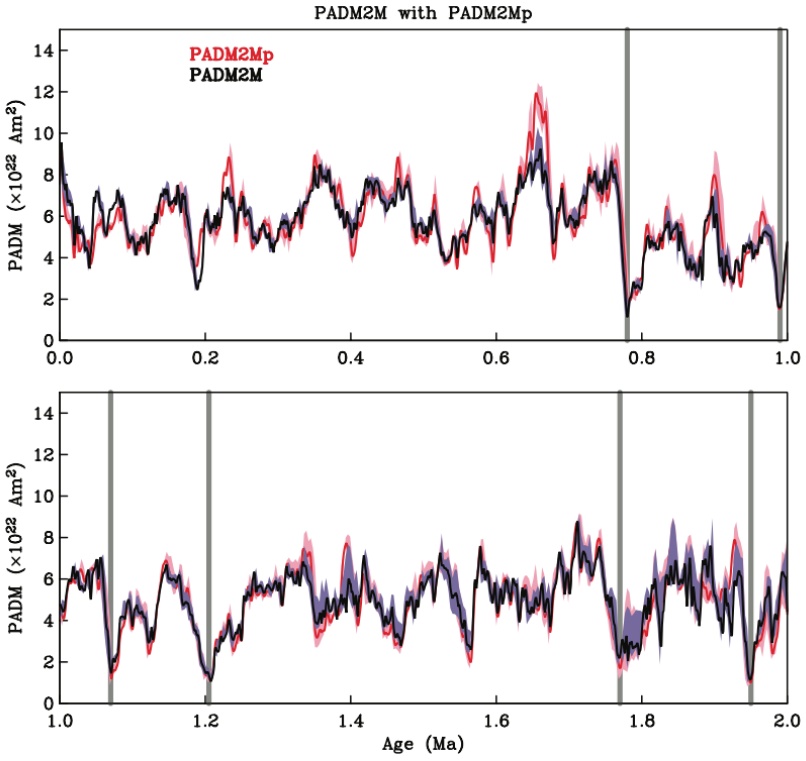

Figure 1.4. PADM2M (black) and PADM2Mp (red) field intensity models for the last 2 Ma (top panel is 0-1 Ma and bottom panel is 1-2 Ma) made by Ziegler et al. (2011). PADM2Mp is a preliminary model produced from nine of the available relative paleointensity (RPI) time series, whereas PDM2M is the model produced from a more complete set of RPI data. Gray vertical bars represent periods of low intensity during known reversals.

that has been constructed from 86 relative intensity records for sediments and more than 5000 absolute intensity estimates from lavas and archeological material. PADM2M uses globally distributed sediment cores to extract relative paleointensity data, and uses absolute paleointensity data for calibration, to approximate the axial dipole moment over the last 2 million years. Today's dipole moment is about $8 \times 10^{22}\ Am^2$ for Earth, corresponding to a surface magnetic field of about 30 μT at the equator, and double that at the poles. It is apparent looking back over the past 2 million years that there have been some large variations in dipole moment. As seen in Figure 1.4 of PADM2M, there seem to be low dipole moments at polarity transitions. This is compatible with work by Clement (2004) that looked at the duration of geomagnetic polarity reversals; It is generally accepted that the field intensity drops to low levels during reversals, typically with a longer period of low intensity (several thousand years) than for directional changes. The PADM2M record will show up again within the results (Chapter 3), as we use this field representation as an input to model remanence acquisition in slowly-cooled intrusions.

1.2 – PSV from large igneous intrusions

Igneous intrusions are large bodies of magma that cool slowly at depth. Similar to lava flows, intrusions acquire a thermoremanent magnetization (TRM) during cooling that can potentially provide useful declination, inclination, and absolute intensity information about the geomagnetic field. Typically, though, data from intrusions have not been used for PSV studies because directional and intensity variations are expected to represent time-averaged field behavior, and the details of how slow cooling affects the time averaging of magnetization in intrusions are poorly understood. Although this averaging would be expected to reduce the directional (and intensity) variations in a large, slowly-cooled intrusion, results from large

intrusions indicate that they may show significant directional scatter. This is illustrated in the comparison below (Figure 1.5) which shows directions from nearly contemporaneous intrusions in Antarctica and lava flows in South Africa. The areas were adjacent and both experienced magmatism associated with the breakup of Gondwana about 180 million years ago. The different average directions reflect plate motions since this breakup, but both types of materials appear to have similar directional variations despite the very large difference in cooling time.

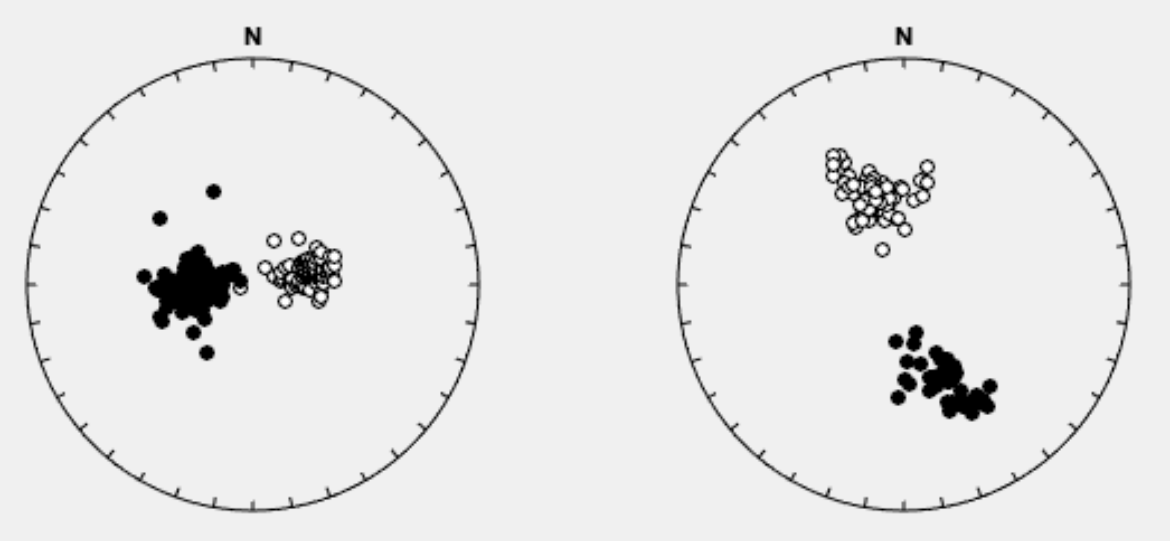

Figure 1.5. Comparison of approximately contemporaneous (~180 Ma) geomagnetic directional variations recorded in slowly-cooled Dufek intrusion (left) and Karoo lavas (right). Differences in average directions reflect plate motion since 180 Ma. Dufek directions represent the highest temperature magnetic component, corrected for remanence anisotropy (k = 91.8, n = 207). Lava directions (excluding transitional directions) are from Moulin et al. (2011) and Kosterov and Perrin (1996) and have k = 58.3 (n = 134). Open circles represent upward directed remanence and filled circles downward directed remanence.

We might expect samples from the Dufek intrusion, which cooled over much longer timescales than the Karoo lavas, to have more tightly clustered directions and a significantly higher kappa value. The Dufek directions are marginally more clustered (k = 91.8, left plot in Figure 1.5) than those of the lavas (k = 58.3, right plot in Figure 1.5) though the difference is small. The directional scatter in slowly-cooled intrusions may also be affected by the properties of the intrusion itself (e.g. strong fabrics within the intrusion, Cheadle & Gee, 2017). Indeed,

these additional contributions to scatter are significant for the Dufek intrusion. The directions shown for the Dufek intrusion have been corrected for remanence anisotropy; the uncorrected directions (n = 249, k = 31.6) are actually more scattered than for the lava samples though again the difference is small. The source of these differences in dispersion is not particularly well understood though both the smoothing from slow cooling and any properties of the intrusion that might affect the remanence must be considered.

Although slowly-cooled intrusions are available throughout Earth's history and so might provide valuable additional information on geomagnetic field variations, very few papers have examined directional variations from large intrusions in terms of characterizing PSV. There have been a few attempts at using slowly-cooled intrusions to examine time-varying geomagnetic field behavior, predominantly looking at polarity reversals. Dunn et al. (1971) and Dodson et al. (1978) identified dual polarity magnetizations in the Miocene Tatoosh intrusion in Washington and argued that intrusions should provide a continuous, potentially high-resolution record of field variations during a polarity transition. The Tatoosh records two reversals, which Dunn et al. (1971) show are not related to reheating or mineralogical changes. The systematic pattern of normal and reverse polarity samples relative to a proposed cooling front in the intrusion provided further support that the magnetizations record a polarity transition during initial cooling. Dual polarity magnetizations have also been documented from the Bushveld Complex, the largest known mafic layered intrusion (Letts et al., 2009; Cawthorn and Webb, 2013). The ~2054 Ma Bushveld complex is approximately 8 km thick, and exposures span more than 250 km, resulting in a volume of ~10^6 km^3. Based on more than 100 sampling sites distributed across these exposures, Letts et al. (2009) were able to define a composite polarity sequence with up to eight polarity intervals. Pechersky et al. (2004) conducted perhaps the most comprehensive attempt to

reconstruct a time series of field variations from several large, Precambrian intrusions. They combined a conductive cooling model with thermal demagnetization data to provide a temporal record of declination and inclination variations. These authors also argue that such studies should provide a continuous record of field variations during cooling, and they find that the resulting secular variation is similar to that of the Cenozoic.

Paleointensity studies from large intrusions that have silicate-hosted magnetite have been used to characterize intensity fluctuations. When magnetite is present as elongate grains it can possess single domain like (the properties of single domain particles will be discussed below) characteristics, which makes it a good recorder of past magnetic field variations. Mafic intrusive rocks often have discrete, high unblocking temperature spectra that differ from lava flows. The fact that the magnetite grains are included in other silicate minerals also means these grains are less likely to alter during the multiple heatings that are necessary to estimate the ancient field intensity (and direction). This makes intrusions well suited for preserving records of the magnetic field through geologic time. Selkin et al. (2008) looked at the distribution of site-mean paleointensities from the 2.7 Ga Stillwater Complex, a large mafic intrusion in Montana. They argued that large, slowly cooled mafic intrusions should provide a good estimate of the average intensity during cooling due to the high coercivity (resistance to changes in magnetization) and discrete unblocking 550°C - 580°C remanence attributed to silicate-hosted magnetite in plagioclase-rich rocks. Their thermal model suggests that the intrusion took 50,000 - 200,000 years to cool from 580°C to 550°C if cooling was purely conductive. The cumulative distribution of intensities was compared to more recent intensity variations, and the authors found that the distribution is compatible with slow cooling thermal models and with secular variation similar to that of the Phanerozoic (Selkin et al., 2008). They interpret the similar paleointensity

distributions to reflect a lack of long-term (~1 billion year) trend in Earth's average dipole moment.

1.3 – Potential PSV records from the Dufek intrusion

Although there have been some promising results in terms of using intrusion records to study geomagnetic field variations, one motivation for the current study is that we still don't understand how measures of PSV are affected by slow cooling. For that reason, it would be useful to have access to high density paleomagnetic sampling through an intrusion that records multiple polarity reversals. The Dufek, a large igneous intrusion in Antarctica that was emplaced at a high southern latitude (~52°S) about 182 million years ago, provides detailed paleomagnetic data, as it has been densely sampled throughout its stratigraphic profiles. Early reconnaissance sampling in the intrusion revealed the presence of both normal and reversed polarity samples (e.g. Beck, 1972), though no sampling section had more than a single N and R polarity. In the Austral summer of 2006/2007, 630 oriented rock cores were derived from the lowermost 600m of the section. The detailed sampling and the presence of dual polarities provides a good data set to examine smoothing of the geomagnetic signal during slow cooling.

An additional feature of the Dufek intrusion is that its cooling history occurs during a period called the Mesozoic Dipole Low (MDL), a term coined by Prévot et al. (1990) for the period from ~180 to 120 Ma thought to be characterized by low intensities and a high reversal rate. The Dufek could provide insight into whether geomagnetic field reversals are correlated with intensity as well as potentially addressing whether such low intensity intervals might be accompanied by increased directional scatter.

Understanding the timescale of cooling of large intrusions can help to link the extracted paleomagnetic data to geomagnetic behavior. As described above, mafic intrusions that have remanence primarily carried by fine-grained, silicate-hosted magnetite, which the Dufek does, are able to capture the magnetic field present at a point in time as the rock cools. Since slow cooling provides some smoothing of the field, we try to understand and quantify the degree of smoothing to link the results from slowly-cooled intrusions to geomagnetic field behavior in the past. Most of the studies surrounding the MDL don't provide sufficient evidence to fully characterize the geomagnetic field, as much of the MDL predates the best-documented magnetic anomaly record from the seafloor and magnetostratigraphic records are sparse. Paleointensity data from the heavily sampled Dufek could provide some degree of averaging that should yield better estimates of the time-averaged field intensity.

Perhaps the largest source of uncertainty in trying to derive temporal record from large intrusion is the time scale of cooling and blocking of the remanence The largest known layered intrusion on Earth, the ~2054 Ma Bushveld complex in South Africa, is a well-studied intrusion that provides some bounds for likely cooling times for large intrusions. Mineral compositional variations within the complex constrain the likely volumes of additions to the magma chamber, allowing a detailed thermal model to be constructed (Cawthorn and Walraven, 1998). These models suggest that the complex required approximately 180 kyr to completely crystallize, and that cooling times from 580°C (Curie temperature of magnetite) to about 500°C ranged from ~100 kyr near the top of the intrusion to a several hundred kyr in the lower portion of the intrusion (Figure 1.6; Cawthorn and Webb, 2013).

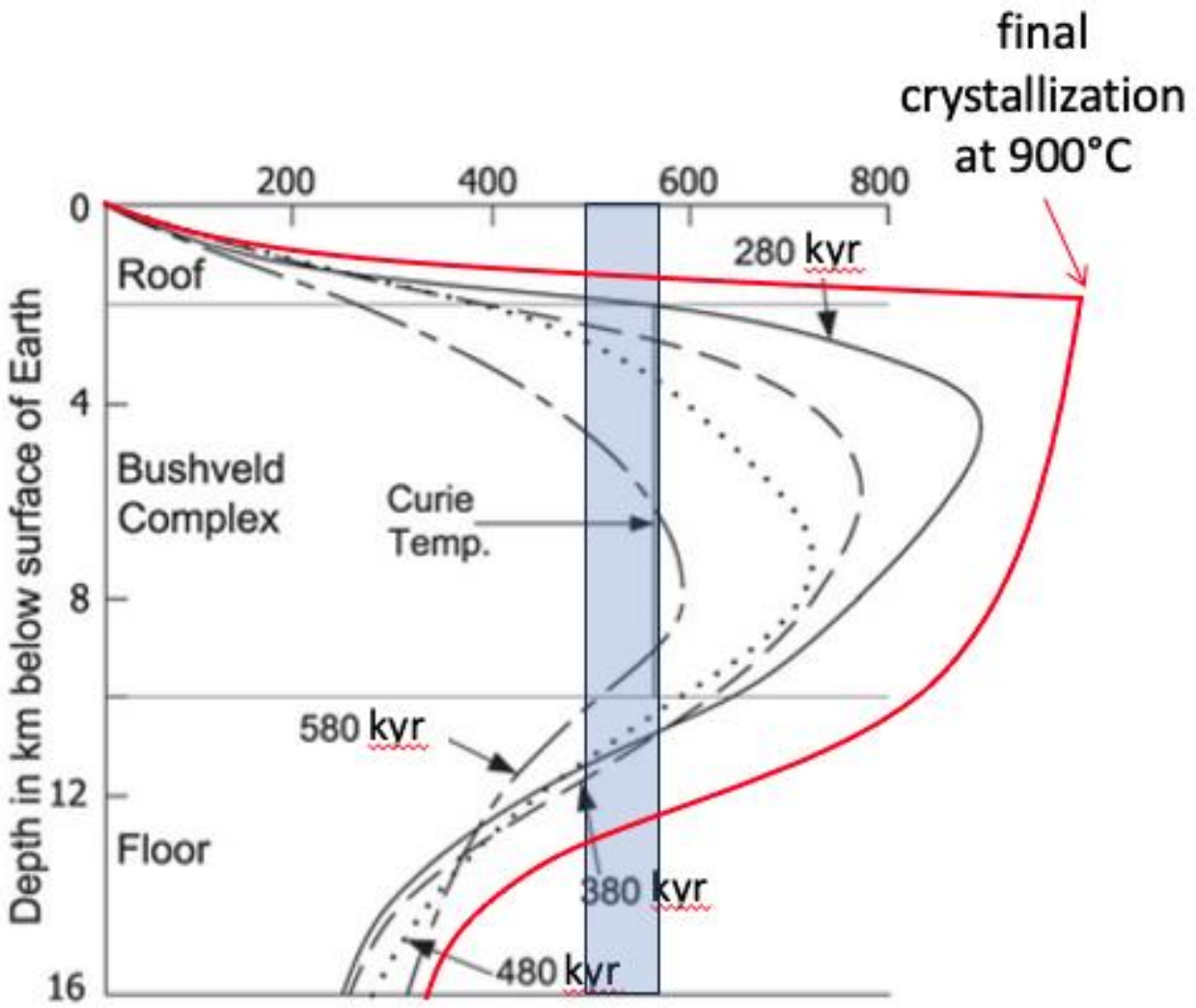

Figure 1.6. Cooling regime of the Bushveld complex (after Cawthorn and Webb, 2013). The temperature distribution (°C) at the time of final crystallization is shown by the red line with additional temperature profiles (black lines) spanning approximately the first half million years of cooling. The blue bar indicates the dominant blocking temperature range for samples from the intrusion, from the Curie temperature of magnetite (580°C) down to about 500°C.

As previously mentioned, Selkin et al. (2008) found an upper limit of around 200 kyr for cooling down to 500°C within the Stillwater, which is about 6600 km^2 in areal extent (volume of ~52,000 km^3 assuming a thickness of 8 km). Both Bushveld and Stillwater intrusions can take a few millions of years to cool completely. We can give an estimate of cooling for the Dufek by referring to these previous studies on big, layered intrusions such as the Bushveld or Stillwater

Complex. As outlined by Ferris et al. (1998), the Dufek and Stillwater are thought to have similar area extents, although Behrendt et al. (1980) suggested that if the Dufek and its neighboring Forrestal Range are part of the same intrusion, its maximal areal extent could be 50,000 km^2 (volume ~450,000 km^3, assuming minimum 9 km thickness for the combined Dufek and Forrestal), which is more comparable to the Bushveld. We can approximate the Dufek's cooling times down to 500°C to be on the same order as these intrusions and in the modeling that follows we examine a variety of cooling times that might be representative for the intrusion.

Thermal demagnetization data from the Dufek intrusion (Gee, unpublished data) reveal the presence of samples with one, two, and three well-defined magnetization components (Figure 1.7.a) in the lower portion of the Dufek. The lowermost ~500m exposed in the Dufek intrusion preserves a record of multiple (minimum of 4) polarity intervals (Figure 1.7.c) and low field

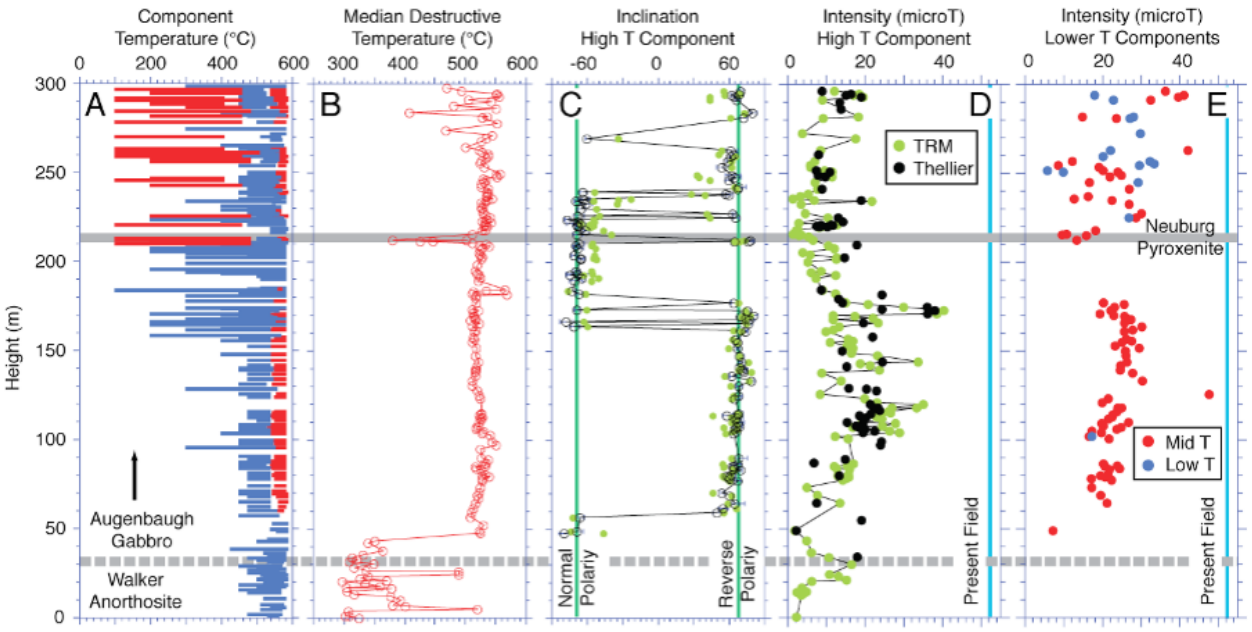

Figure 1.7. Paleomagnetic results from lower portion of the Dufek Massif sampled during the 2006-07 field season. (a) Component temperature illustrating the unblocking temperature range of reverse (red) and normal (blue) polarity components. (b) Median destructive temperature is the temperature at which 50% of the remanence remains. (c) The inclination of the highest temperature components (solid green = observed; open = corrected for remanence anisotropy). (d) Intensities for highest temperature component estimated from Thellier double heating and TRM demagnetization technique. (e) Intensities for intermediate and low temperature components estimated by the latter technique. Note that all intensities are low compared to the present field intensity (vertical blue line).

intensity. In many cases, this is comparable to values found during excursions or reversals. Paleointensity estimates from the Dufek reveal serially correlated and remarkably low values (average ~14 μT, about one quarter of the value expected from today's field value for a paleolatitude of 52°S), with less variable intensities for lower temperature components, which might be expected from slower cooling at these lower temperatures. Together with several additional reversals documented at higher stratigraphic levels, this is suggestive of a weak (perhaps fibrillating) field that differs markedly from more recent records of the geomagnetic field.

1.4 – Outline of goals

This thesis aims to decrease the knowledge gap between PSV and recorded intensities by characterizing how the slow cooling process in intrusions affects how the time varying field would be recorded, e.g. by examining the effects of slow cooling on the remanence preserved. In addition to cooling times, we require information on how remanence acquired during slow cooling relates to the remanence acquired over laboratory time scales. For this, we use the single domain (SD) cooling code produced by Nagy et al. (2021). This code models the acquisition of thermoremanence in uniformly magnetized SD particles (commonly referred to as Stoner-Wohlfarth particles; Stoner and Wohlfarth, 1948) and provides both a theoretical basis for looking at the effect of cooling rates on remanence and a way to forward model remanent magnetization in slowly-cooled intrusions. This code was developed to track the acquisition of blocked remanence for a population of SD particles where the magnetic energy is determined

only from the magnetostatic energy of the particles (i.e. magnetocrystalline and magnetostriction contributions to these energy barriers are not considered, and shape is the dominant anisotropy). Fortunately, these constraints are likely adequate for the elongate, SD-like grains (typically hosted within silicate grains) that are the dominant remanence carriers in layered intrusions.

The SD code could be modified to model a particular distribution of grain sizes during cooling in a time-varying field, but we opted for an implementation that allowed more general tests to be performed. Specifically, we calculated the remanence blocked over a series of cooling times (1 kyr, 10 kyr, 100 kyr for the rock to cool from 580°C to 500°C) and for a range of grain sizes (from 20 nm to 85 nm), and then we use these results, combined with an estimated grain size distribution, to model the remanence expected for samples within a stratigraphic section of a large intrusion. This approach allows us to examine a large range of models that represent blocking of remanent magnetization under a variety of conditions (e.g. cooling rate, time-varying field), and for a variety of rocks with different grain size distributions.

We use these models, and data from the densely sampled Dufek intrusion, to characterize the smoothing/filtering of the geomagnetic signal that is inherent in remanence records acquired during slow cooling. We first go through a series of simple tests, with a modeled constant field and a simple reversal, that provide useful information about cooling at different time scales to help characterize PSV. From these results we also simulate the behavior during laboratory thermal demagnetization to facilitate comparison with this common type of paleomagnetic data. Other tests involve both statistical field models and Earth-like models. We find that existing statistical models of geomagnetic variability, such as CJ98 (Constable and Johnson, 1999) that is based on directional variation in lavas over the past 5 million years, result in magnetizations far smoother than observed in intrusions, since they are not correlated in time. We also explore

combining the directional variations of CJ98 with reconstructions of axial dipole moment variations (PADM2M, Ziegler et al., 2011) but these likewise produce only subdued directional variations in the modeled intrusion.

A more Earth-like model, such as the Geomagnetic Global Field model spanning the past 100 kyr (GGF100k, Panovska et al., 2018), has temporally correlated variations that can help quantify the amount of smoothing we see in slowly-cooled intrusions. Short excursions of low intensities can even be recognized in the modeled remanence of the intrusions at various cooling timescales. These results will serve as a first step towards understanding how slowly-cooled, large igneous intrusions can serve as a means for characterizing PSV, as our model can give a good representation of variability recorded over cooling and may allow a geomagnetic signal to be recovered from large intrusions, therefore broadening our understanding of the dynamics of the geomagnetic field throughout time.

Chapter 2 METHODS

One approach to understanding more complex relationships within the paleomagnetic realm is to use simpler scenarios that can still allow us to explore key aspects of the recording process in slowly cooled intrusions. We use the single-domain (SD) modeling code of Nagy et al (2021), hereafter referred to as *sd-cooling*, to calculate the cooled (blocked) magnetization of an assemblage of identical particles for a range of grain sizes and various cooling times. The data for individual grain sizes can then be combined to match the blocking temperature/grain size distributions of the intrusion samples to be modeled. By using pre-calculated blocking curves, we are able to efficiently explore a range of time-varying geomagnetic field models and how these are recorded in the samples. This code is publicly available through Lesleis Nagy's github repository (see https://github.com/Lesleis-Nagy/sd-cooling).

The ability of magnetite (or any other magnetic mineral) to preserve a record of past magnetic field is explained by the Stoner and Wohlfarth model (Stoner & Wohlfarth, 1948). It rests on the fact that certain "easy" directions provide lower energy states for the grain magnetization. There are several possible sources of anisotropy that may produce "easy" and "hard" directions but perhaps the simplest one to visualize is shape anisotropy (Figure 2.1). For minerals like magnetite with a high spontaneous magnetization, even a slight elongation of the grain will result in an "easy" axis directed along the long axis of the grain. So there are two potential "easy" directions, one pointed in either direction along this "easy" axis. At high temperatures thermal fluctuations are sufficient to cross the energy barriers separating these two "easy" directions. As temperature falls, the energy barriers grow and the magnetization will be trapped into one of the two easy directions and the presence of an external field during cooling results in lower energy for one of these "easy" directions (the one closest to the field direction).

If a sample has many such grains with randomly oriented "easy" axis directions, this energy difference between the two states results in a small (typically ~1%) statistical alignment parallel to the field. For a given grain size of single-domain particles this locking in of the magnetization, called blocking, happens over a small temperature range.

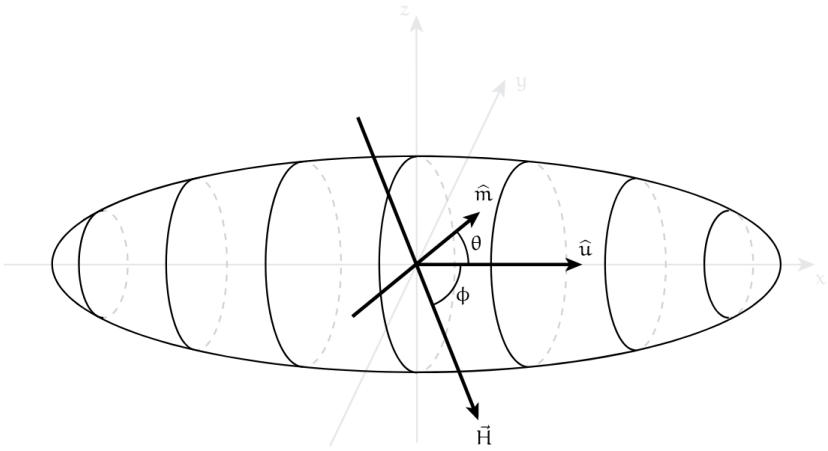

Figure 2.1. From Nagy et al. (2021) the simple Stoner-Wohlfarth model shows an ellipsoid grain oriented along the vector $\hat{u}$ with an applied field H. The magnetization m makes angles and with $\hat{u}$. The magnetization will rotate within the $\hat{u}$ - H plane. For an arbitrary angle , there will always be a three dimensional magnetization vector.

Large intrusions, such as the Dufek, can have remanence that is dominated by silicate-hosted magnetite particles that occur as small (a few microns in length) elongate inclusions in plagioclase and pyroxene (e.g. Ageeva et al., 2020, Cheadle & Gee, 2017) that are similar to ideal single domain (SD) particles. Although contributions from magnetocrystalline and stress are not considered in the *sd-cooling* model, the code is well suited for the elongate populations of magnetite grains hosted within silicate grains. The distribution of grains within the model that get magnetized along their “easy” axis can simulate a mafic rock with silicate-hosted magnetite. As described in previous sections, this is not too far from realistic in our case; the presence of these elongate magnetite grains can be typical for many large mafic intrusions. These

characteristics suggest that the magnetite properties of intrusions should be well modeled as elongate grains.

The *sd-cooling* code is based on Néel's theory (Néel, 1949) for thermoremanence magnetization (TRM) in uniformly - magnetized (single domain) particles. The code minimizes the magnetostatic magnetic energy for a population of grains during cooling in an applied field. Equation 2 demonstrates the minimization of energy;

$$\text{Equation 2: } E(\theta,T) = C_1(T)sin^2\theta - C_2(T)cos\theta - C_3(T)sin\theta,$$

where θ is the angle between the unit magnetization vector m and the grain axis u, as seen in Figure 2.1, and $C_1(T)$, $C_2(T)$, and $C_3(T)$ are temperature dependent constants represented by;

$$C_1(T) = \frac{1}{2}(N_b - N_a)v\,\mu_0\,M_s(T)^2,$$

$$C_2(T) = H\,v\,\mu_0\,cos\phi\,M_s(T),$$

$$\text{and } C_3(T) = H\,v\,\mu_0\,sin\phi\,M_s(T),$$

where $M_s(T)$ is the saturation magnetization at temperature T, μ_0 is the permeability of free space with volume v, H is the externally applied field, and ϕ is the angle between the applied field and grain axis. N_a and N_b are the demagnetization factors along the long and short axis, and depend on the aspect ratio of the grain, e. Nagy et al. (2021) chose to express the elongation as a percent value rather than a ratio. Thus, *percent elongation* is given by $(100e) - 100$. Within *sd-*

cooling, the elongation is specified using a 'value' and a 'fraction'. For example, a fraction = 1.0 and elongation value = 300 corresponds to all grains having an elongation of 300%, or more familiarly a 4 to 1 ratio of long to short axis which is in the correct range for elongate magnetite needles observed in the Dufek rocks. These can range from a micron or two in length, to perhaps 10s of microns in length, and can be a micron or less in width.

2.1 – Defining input parameters for sd-cooling

Defining our desired input parameters for *sd-cooling* was straightforward; We curated a json file (JSON syntax consists of name/value pairs) of inputs to *sd-cooling* corresponding to a set of grain size and cooling timescale parameters. Within that file are the bulk of key identities for each grain size we run. Figure 2.2 represents the important factors from one of the json files we used. A full example file can be found within the appendix (Appendix 1). It's separated into six parameter blocks defining the "material", "sizes", "elongations", "directions", "applied field", and "cooling regime" for the model run.

```
{
  "material": "magnetite",

  "sizes": {
    "list": [{"value": 85, "fraction": 1.0}],
    "unit": "nm"
  },

  "elongations": {
    "list": [{"value": 300, "fraction": 1.0}]
  },

  "directions": {
    "distribution": {
      "type": "fibonacci",
      "nbins": 100
    }
  },

  "applied_field": {
    "strength": 30,
    "direction": [1,1,1],
    "unit": "uT"
  },

  "cooling_regime": {
    "ambient_temperature": 15.00,
    "initial_temperature": 579.999,
    "reference_time": 1.7E14,
    "temperature_at_reference_time": 15.15,
    "allowable_percentage_drop": 0.01,
    "stopping_temperature": 50
  },
```


Figure 2.2. Example json file that is used to establish the magnetic material, grain size, elongation percent, number of bins, field strength and direction, and cooling properties. This file was used for the longest time scale of 100,000 years, and so has a reference time of 1.7E14. It was also for the largest grain size of 85 nm.

For all samples, some of the components remain the same – we've set magnetite as the material, 300% as the elongation, 30 μT for the applied field strength, a field direction of [1,1,1], and an allowable percent drop of 0.01%. An explanation for these selected values is discussed in the following sections.

Within the cooling properties, we always kept "initial temperature" at 580°C and "stopping temperature" at 50°C. Different grain sizes were tested for each timescale, ranging from 20 nm to 85 nm. The blocking temperatures observed in the Dufek samples typically extend from ~500°C to very close to the Curie temperature of magnetite (580°C). We chose the largest

grain size to produce laboratory unblocking near the Curie temperature: 85 nm gives laboratory blocking temperature of about 577°C. Although most of the blocking in the rocks we're modeling occurs above 500°C, we extend the output cooling data down to 50°C to allow for all the grains to get blocked. The smallest grains can have large blocking temperature ranges at low temperatures (e.g. 20 nm grains for slowest cooling spans from 87.9° to 49.9°C).

Within the cooling regime section of the json file, there is also "reference_time". This refers to the total time it takes a sample to cool from 580°C to 15.15°C. Possible reference times were chosen based on the desired time it took samples to cool from 580°C to 500°C, where the bulk of the remanence of samples from the Dufek (and many other mafic intrusions) gets blocked. For example, we calculated cooled remanence for all grain sizes for three slow cooling time scales (1 kyr, 10 kyr, 100 kyr to cool from 580°C to 500°C) as well as cooling over laboratory timescales. These timescales correspond to 580°C to 50°C 'reference times' of 6.0E3 seconds, 1.7E12 seconds, 1.7E13 seconds, and 1.7E14 seconds, and that is what we used as our reference time in *sd-cooling*. Figure 2.3 demonstrates how the reference cooling time exponents correspond with the desired 580°C to 500°C cooling.

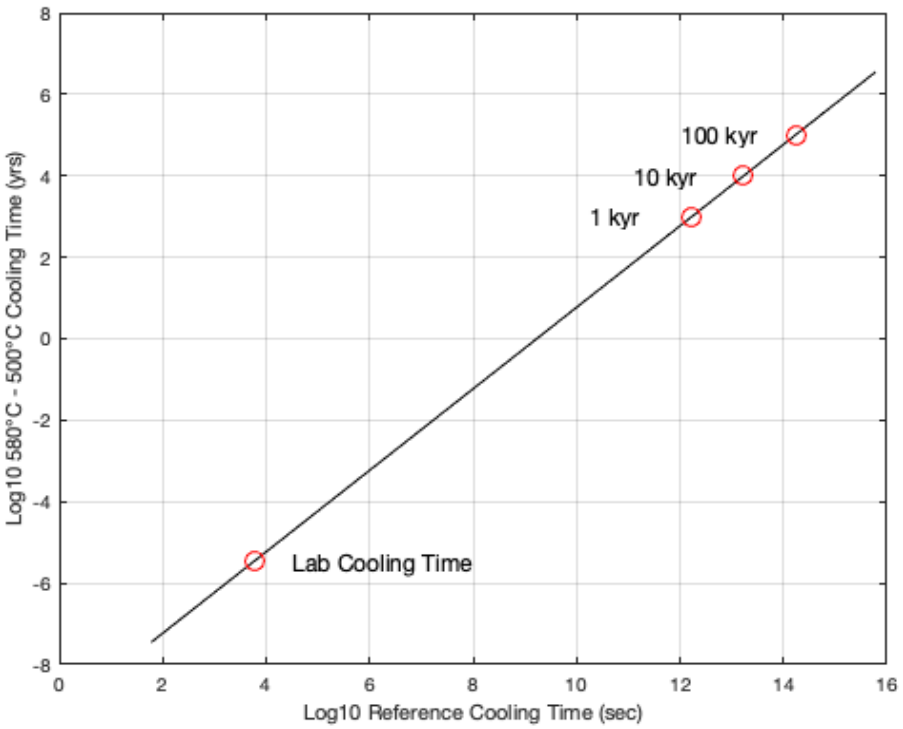

Figure 2.3. Reference cooling time represents the time it takes for a distribution to cool from the initial temperature (580°C) to the stopping temperature (50°C). The reference times represented are 6.0E3 seconds, 1.7E12, 1.7E13, and 1.7E14. These correspond to cooling times for 580°C down to 500°C of lab timescales, 1 kyr, 10 kyr, and 100 kyr. The reference times are plotted on the graph, and are labeled with their respective 580°C to 500°C cooling times.

For *sd-cooling* to compile properly on our local computers, we needed to have a Boost library (version 1.76.0) and a CMake platform (3.17) that was compatible with the code. The University of Liverpool had compatible versions of Boost and CMake available on their systems, and graciously allowed permission to use their supercomputer to compile and run the *sd-cooling* code. To simplify how we characterize each grain size at each cooling timescale, we created shell scripts that would step through each grain size we wanted at each reference time. In our case, that meant going from 20 nm to 85 nm for four different timescales. After completing an ssh to access the University of Liverpool supercomputer through a terminal window, the scripts got called in to set up the directories for all the grains and timescales. Then, a shell script with

SLURM commands would get submitted to the queue on the supercomputer to run the code with our chosen characteristics. SLURM is a workload management system that is often used in supercomputer environments where multiple cores can be used. An example directory with all the files needed to run one sample can be found in the appendix (Appendix 1).

The resulting cooled remanence for each assemblage should, ideally, be independent of the applied field direction if a sufficient number of grains are used and if their easy axes are uniformly distributed on the unit sphere. The standard 1" diameter cores used in many paleomagnetic studies will contain a very large number of magnetic grains, ensuring that the laws of statistical thermodynamics (Maxwell-Boltzman statistics) inherent in modeling single-domain remanence acquisition are applicable (e.g. Berndt et al., 2015). It is impractical to compute remanence for large numbers of grains and so *sd_cooling* uses a much smaller assemblage of grains and a spatial Fibonacci distribution (see for example Roberts, 2020) to approximate a uniform distribution of easy axes on the unit sphere.

Figure 2.4 illustrates the distribution of easy axis directions generated by *sd-cooling* for Fibonacci distributions with 30 and 100 grains. In both cases, the distribution of axial directions is relatively uniform over the sphere but not perfectly so. To characterize the degree of uniformity we calculated the minimum angular difference for each direction to its nearest neighbor. For a population of 30 directions, the median angular difference is 35.2° with an overall range of 32.7°-37.2°. For a population of 100 directions, the median angle to the nearest neighbor is 19.4° with an overall range from 17.8° to 19.7°.

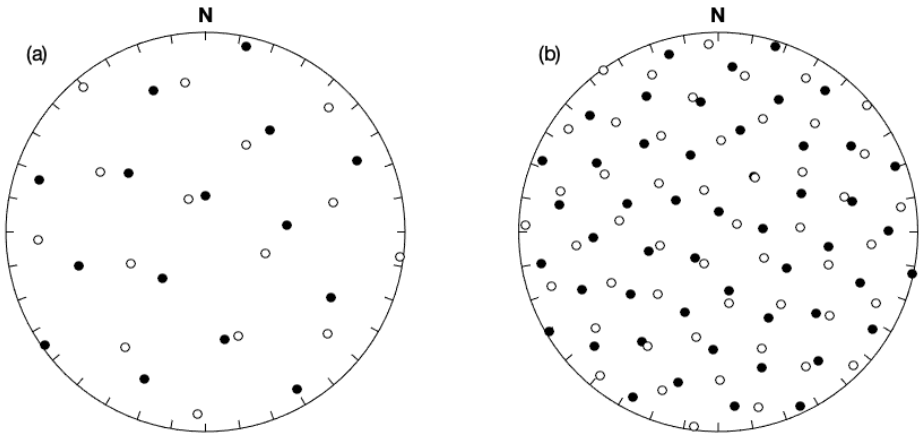

Figure 2.4. Equal area plot showing approximately uniform distribution of grain easy axes for Fibonacci distributions of a) 30 and b) 100 grains. Filled circles indicate lower hemisphere directions and open circles indicate upper hemisphere directions.

Our initial runs compared the cooled remanence acquired in different applied field directions to evaluate whether the small number of grains in the Fibonacci distributions are sufficient to yield results that are independent of the applied field direction. These tests were done with a population of 30 grains, each 50 nm in size with 100% elongation and a reference cooling time of 3.5E12 seconds (corresponding to a cooling time of 2 kyr from 580° to 500°C). The field intensity was constant (30 μT) and directed along north [1,0,0], east [0,1,0] or down [0,0,1] or at an intermediate [1,1,1] direction corresponding to a field direction of 045°/35°. Nagy et al. (2021) notes that however the direction is specified, it will always be normalized to be a unit vector. The final cooled remanence for these four applied field directions barely varies, as shown by Figure 2.5.

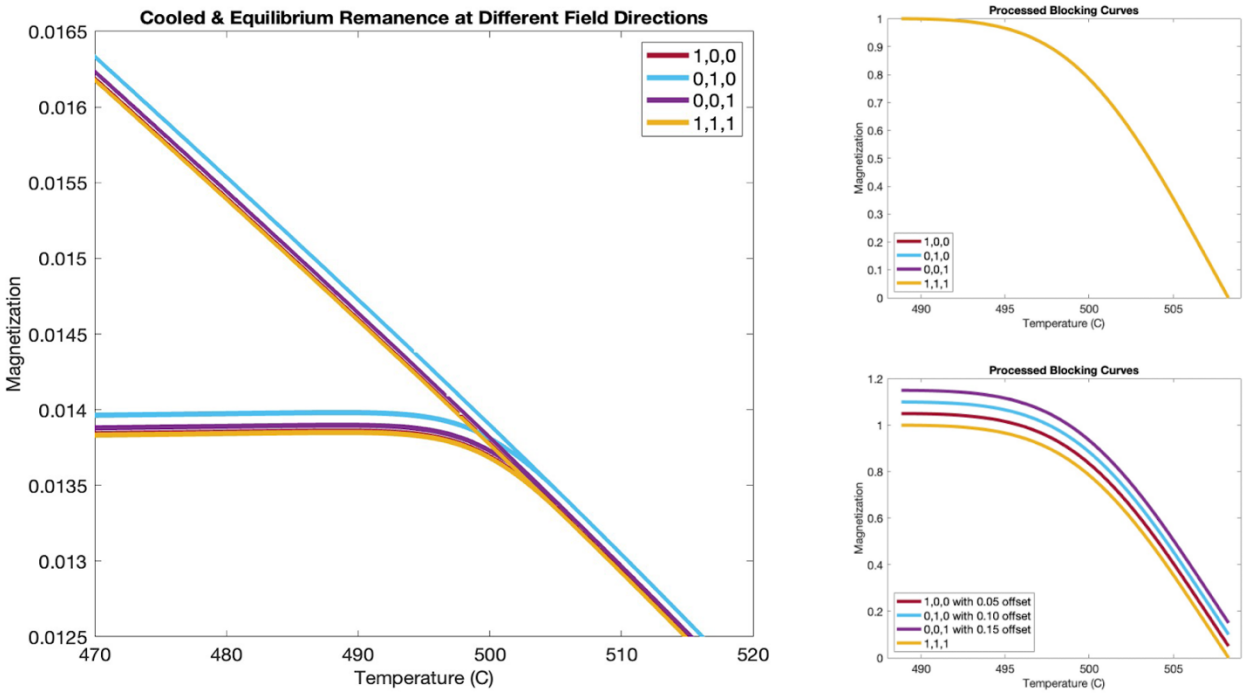

Figure 2.5. Comparison of different applied field directions for cooled and equilibrium curves. Right graphs demonstrate the cooled and equilibrium curves after processing, normalized to 1. Each direction in the lower right has been given an offset to visualize the similarity in curves. With no offset, as seen in the upper right, only the [1,1,1] direction is visible since each curve is overlaid by the other. Each test was run with a grain size of 50 nm, near the mean of the 20-85 nm size range modeled. Although there is some variability for the field directions, the processed data shows they will act the same within our model, so going with one direction will not hinder anything.

The shapes of the blocking temperature curves, as well as the temperatures at which blocking begins and ends, are nonetheless quite similar (Figure 2.5). The similarity of the normalized blocking curves suggests that the Fibonacci orientation distribution is sufficiently uniform to be relatively insensitive to the applied field orientation, i.e. the distribution of orientations is large enough and uniform enough that cooled magnetization is independent of the field direction. We used an intermediate field direction [1,1,1] for all model runs.

2.2 – Transitioning output of sd-cooling to MATLAB modeling

In this section we describe how output from the *sd-cooling* code, for a range of grain sizes and cooling rates, is used to construct more compact, two-dimensional magnetization and temperature arrays that can be saved and then re-used for modeling remanence acquisition under a variety of conditions. The following sections will then describe how these arrays are used to construct a forward model of remanence acquisition in an intrusion, which will require additional information on the grain size distribution of magnetite particles in the intrusion, its cooling history, and a model of geomagnetic field variations through time. We begin by describing how the multiple files describing remanence acquisition for a single grain size population for a single cooling rate are analyzed.

Our starting point is the *cooling.csv* file generated from each run with comma-separated values of temperature, elapsed time, equilibrium magnetization and cooled remanence for the population of 100 elongate grains modeled. An example output is illustrated in Figure 2.6. The orange curve is the equilibrium magnetization, which represents the net difference between grains with magnetization components parallel and antiparallel to the applied field (e.g. Dodson and McClelland Brown, 1980), and is shown to increase rapidly below the Curie temperature and then continues to increase at lower temperatures. The blue curve represents the cooled (blocked) remanence for this population of grains. Our first job is to isolate the range of temperature over which this blocking occurs, i.e. where the blue curve begins to deviate from the orange curve to where it reaches the (approximately constant) final blocked magnetization.

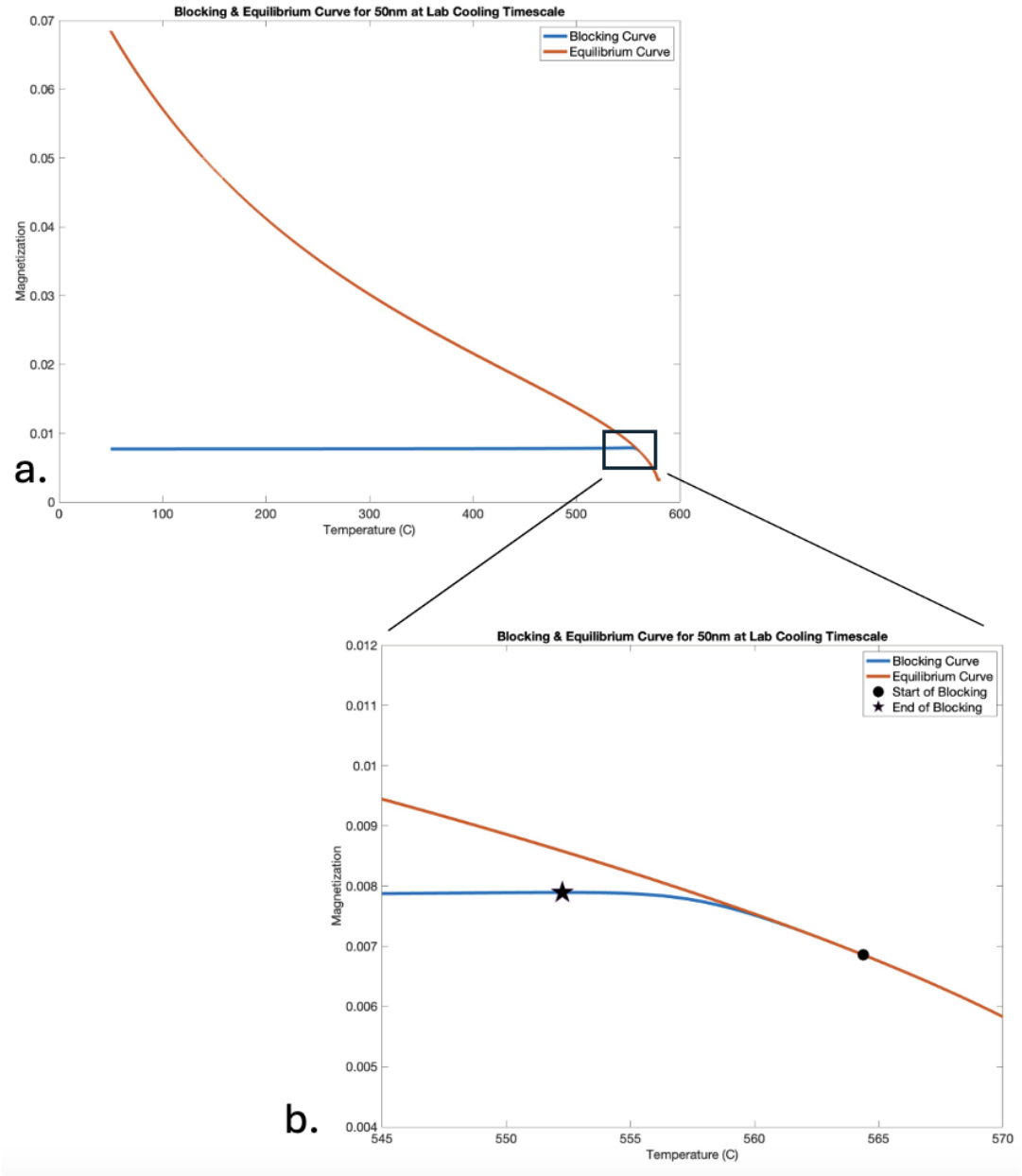

Figure 2.6. Resulting equilibrium remanence and cooled remanence curves as output from Nagy et al.'s model. Graph a) represents cooling down to 50°C, and therefore shows the whole range until cooled. Graph b) demonstrates the start and end of blocking. The start of blocking, represented by a point, begins around 565°C, where the lines start to diverge. There's no visible divergence at that point since the difference in values between curves is within the 14th decimal place. End of blocking, represented by a star, occurs at the maximum along the cooled remanence curve.

A MATLAB subroutine, named 'GetBlocking.m', was made to identify the blocking temperature range and to save the shape and temperature limits of the magnetization curve as the

grain population approached its final blocked magnetization. The temperature at which the two curves deviate (marked with a circle in Figure 2.6) was simple to locate. However, we found there were some points where the blocking and equilibrium curves were flagged as diverging, but a rounding difference in the 16th decimal place caused premature signaling of divergence. This, in turn, caused discontinuous, 'spiky' blocking curves for adjacent grain sizes - the blocking curves should vary smoothly across all grain sizes. To find the proper point of divergence (where blocking begins), we defined epsilon with a value of 1E-14 as a tolerance to allow for small rounding errors. To find where blocking ends (star in Figure 2.6), we found the maximum point along the blocking curve. Why the maximum? Although the cooled remanence curve should theoretically stay constant down to room temperature, there is a slight decrease in magnetization at lower temperatures within the *sd-cooling* model. We used the peak value of magnetization to define the end of blocking to account for the slight dip of the curve, and to ensure we find the point where cooled remanence begins to level off.

Having found the blocking temperature range for a single grain size, our next goal was to save a simplified version of this information for all 66 grain sizes at a single cooling rate. Because the *sd-cooling* code uses a temperature step that is scaled as a percentage temperature drop (more on this below), the number of points on the blocking curve typically varies for each grain size. We wanted to save this information in a two-dimensional array that could be re-used in multiple modeling runs, so we needed to interpolate these onto a uniform number of temperature steps for all grain sizes. We used the same indices (as the point of divergence and maximum) to pull out the corresponding temperature where these samples are getting blocked. We then interpolated to get the magnetization at these 101 points throughout blocking. One might be wondering why we chose 101 temperature step points for our linear interpolation.

Larger temperature steps were causing our linear interpolation to miss some of the actual curve of the line that occurs during blocking. As seen in Figure 2.7, 101 temperature step points and 20 temperature step points seem practically identical from the larger perspective. When zoomed in, though, one can see how using too few points for the linear interpolation does not accurately represent the actual cooled remanence curve.

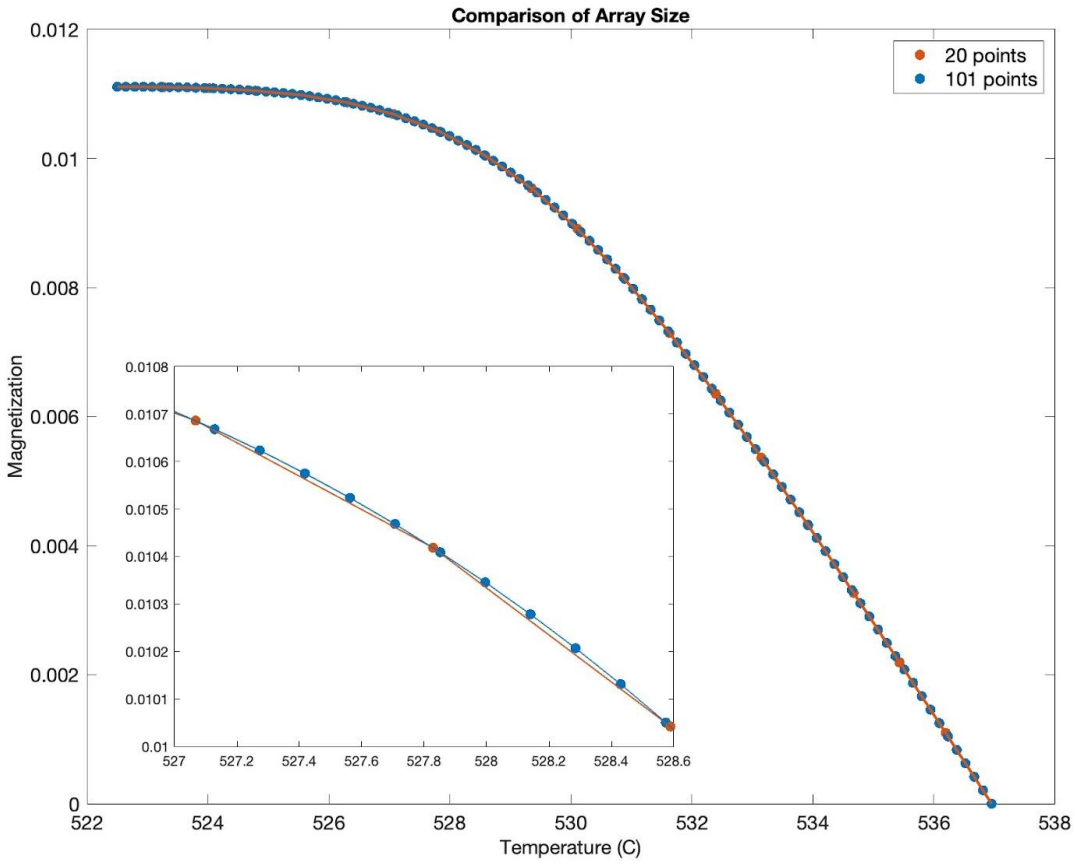

Figure 2.7. Representation of linear interpolation curves with different number of temperature steps to interpolate between. The larger curve has both the 20 point linear interpolation and 101 point linear interpolation plotted on top of one another. The inset plot is a zoom in of the larger curve between 527°C and 529°C. Blue points and the lines in between are characteristic of the 101 point interpolation, whereas the red points and the line connecting them are characteristic of the 20 point interpolation. Although similar, the 20 point linear interpolation is seen to undercut the 101 point interpolation.

One issue we ran into was that we had the "allowable_percentage_drop" set to 0.1% for our initial set of runs. This parameter defines the size of the temperature steps, i.e. how large a

step the model takes as the population cools from 580°C to 50°C. Demonstrated by Figure 2.8, we quickly realized that a 0.1% percent temperature drop from 580°C was giving us too few points within the blocking range for larger grain sizes. This is emphasized by Figure 2.10, as we see the blocking range for large grain sizes at large cooling rates are quite narrow. The linear interpolation using a 0.1% percentage drop does not provide a good representation of the blocking path within this range, so we switched the percent drop to 0.01%. The inset graph in Figure 2.8 shows how the equilibrium curves stay the same for both percent drops, whereas the cooled remanence curve for the larger percent drop makes sharp changes, which are not representative of the slow cooling path of magnetic grains.

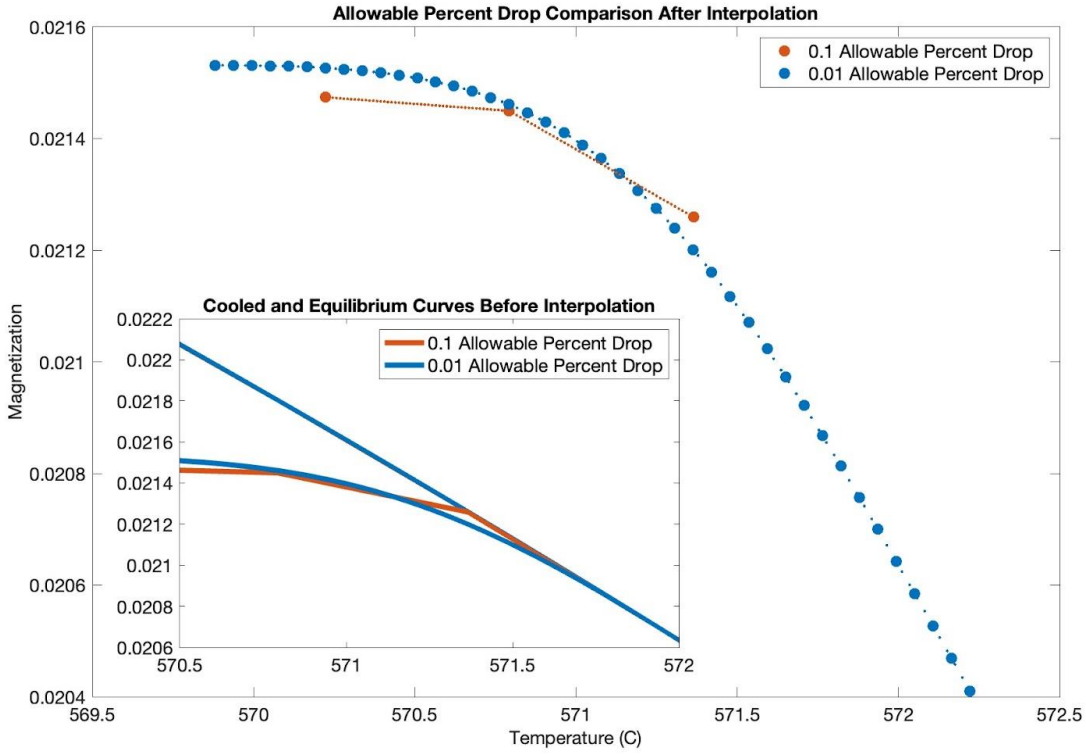

Figure 2.8. Comparison of allowable percentage drop, showing differences between 0.1% and 0.01%. At a cooling time of 100 kyr, for a grain size of 80 nm, there are only three points within the blocking range at an allowable percent drop of 0.1%, whereas the 0.01% percent drop has many more points (40+) and depicts a better determined cooled remanence curve. The inset graph demonstrates equilibrium and cooled remanence curves over the blocking temperature range for both percent drops.

Quick calculations were done to confirm the allowable percent drop was what dictated the size of the temperature step; In *sd-cooling,* all temperatures begin at 579.999°C. For 20 nm at 100 kyr, the second temperature recorded within the initial runs was 579.419°C, which correlated to the 0.1% temperature drop. The re-run sample had a second temperature of 579.941°C, which is 0.01% lower than 579.999°C. Although this effect was only noticeable at larger grain sizes, it was still necessary to rerun all the samples, since the combined blocking curves for different grain sizes had steep changes where the percent drop was different. Rerunning all samples at the same percent drop allowed for a smooth combination of blocking curves at all grain sizes.

The final, simplified output for a single grain size run is the blocking temperature curve. There are two aspects of this curve that are useful. The first is the shape of the blocking curve and its temperature range, and the second is the magnitude of the final blocked magnetization for the grain size population (in our case 100 grains). We combine both these pieces of information as follows. First, we normalized the blocking curve so that it is 0 at the initiation of blocking and 1 for the final blocked magnetization. For example, the onset of the blocking (circle) for the blue curve in Figure 2.6 is set to zero, and the final magnetization (star) is set to 1. This normalized curve represents the increase in blocked magnetization over the appropriate temperature range. This curve is then rescaled so that the final blocked magnetization equals the value of the final plateau on the cooled magnetization curve (e.g. 0.0079 in Figure 2.6).

Now that we've introduced all the components that are needed in understanding why the json file and 'GetBlocking.m' subroutine are set up the way they are, we introduce the summary two-dimensional arrays that are saved for re-use in the intrusion modeling. Within the 'GetMagArrays.m' MATLAB script, we call the 'GetBlocking.m' subroutine to find the values of magnetization for all grain sizes at all cooling timescales. To be able to quickly loop through

each grain size in each timescale, we recommend creating a file with a list of each *cooling.csv* file (which means one for each grain size) per cooling rate. That way, we can easily create two [nsize x 101] (in this case, 66 x 101 because that's how many grain sizes we ran) arrays of magnetization and temperature (for each timescale) during blocking using only one file as the read in. This should be replicated for each cooling rate. Figure 2.9 shows a surface plot of the arrays we get when running 'GetMagArrays.m' for all grain sizes at each timescale. The 'GetMagArrays.m' code only needs to be run once for each timescale, as a csv file can be saved to your computer for use in the later scripts. This just serves to organize the output from *sd-cooling* in a way that prepares the input needed for the rest of the modeling.

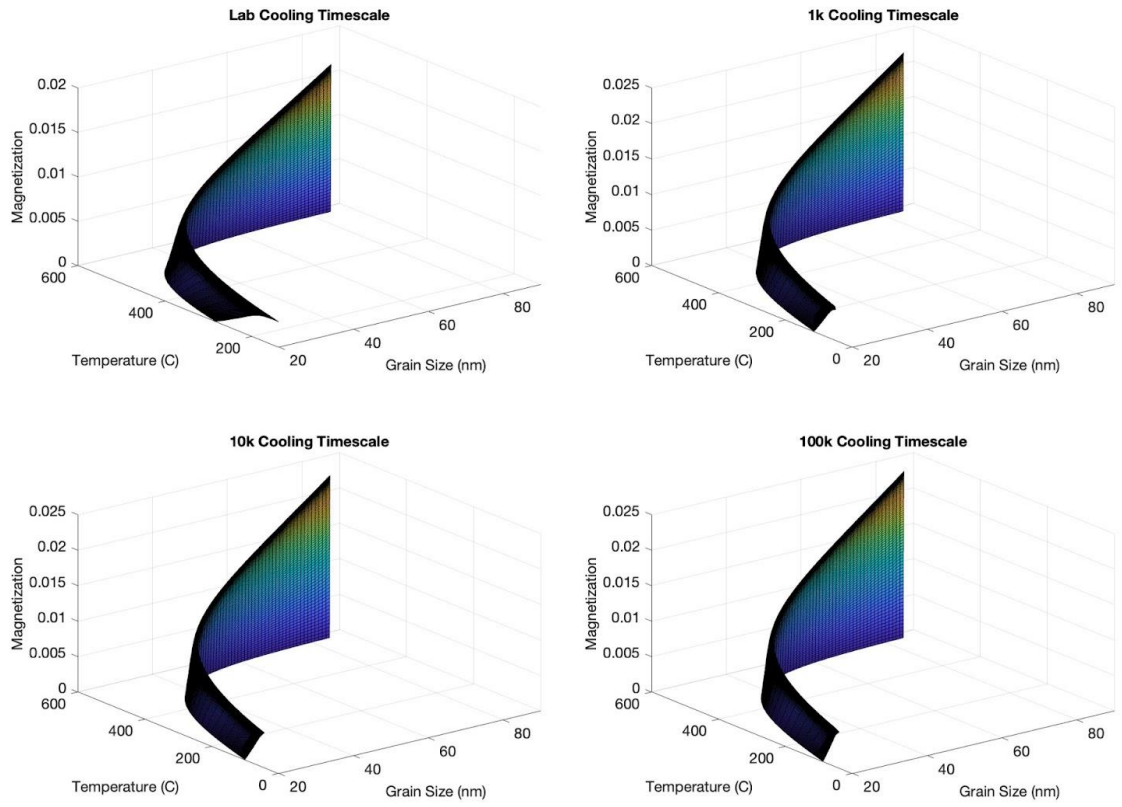

Figure 2.9. Representative surface plots showing magnetization curves (as a function of grain size and temperature) for each respective timescale of cooling. This figure shows the smooth curve we get after making new interpolated arrays from the start of blocking to the end.

Notice in Figure 2.10 that at larger grain sizes, we have narrower temperature ranges where samples get blocked and vice versa at smaller grain sizes where we have a broader blocking temperature range. This is because larger elongate grains have larger energy barriers to overcome, and only higher temperatures have enough energy to cause the grain moments to reorient before being blocked. Smaller grains in turn have smaller energy barriers, meaning there will be a larger temperature range at lower temperatures for these grains to become blocked.

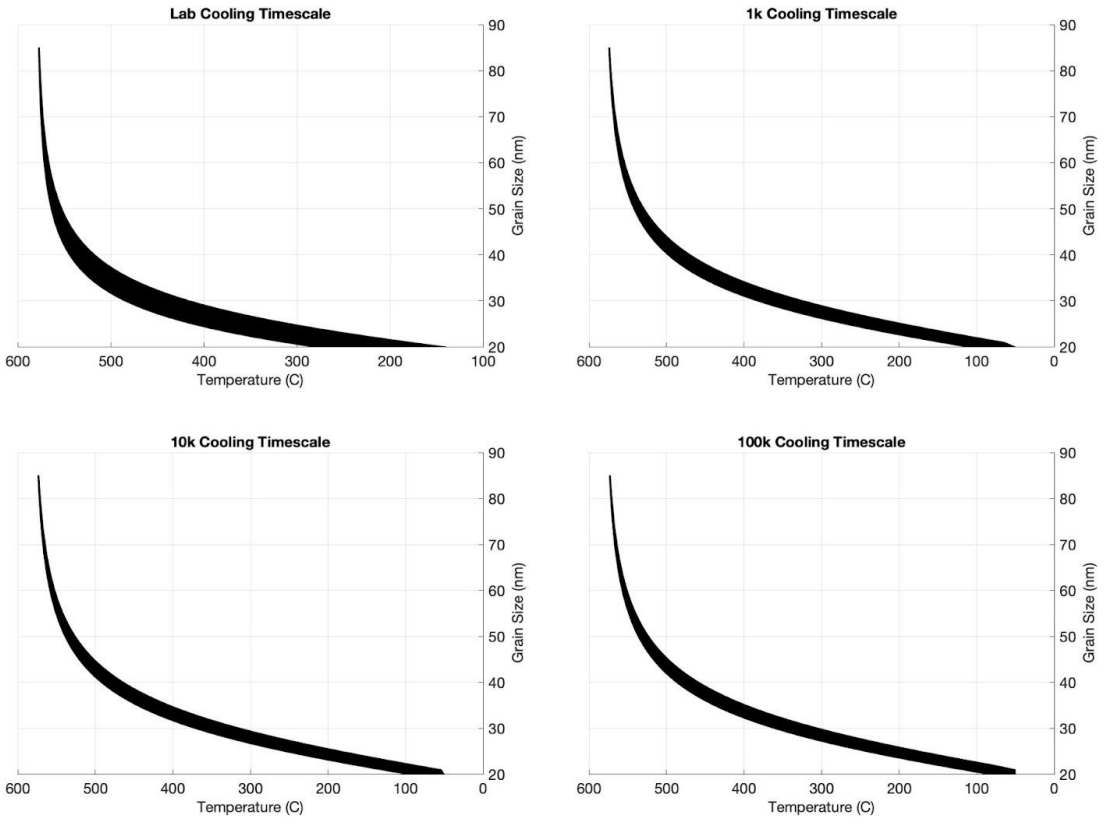

Figure 2.10. Blocking curves with temperature on the x axis and grain size on the y axis. The thickness of the black line indicates the range of blocking temperatures for each grain size. Larger grain sizes get blocked at higher temperatures and have smaller temperature ranges. As temperature decreases during cooling, the smaller grain sizes get blocked accordingly, but have a wider range of blocking.

2.3 – Mapping slowly-cooled remanence to laboratory time scales

Our modeling of remanence acquisition in a slowly-cooled intrusion will ultimately be guided by comparison with laboratory thermal demagnetization data of samples from large igneous intrusions. These natural samples have acquired a TRM during slow cooling. Laboratory studies necessarily begin with measurement of the final TRM at room temperature, and then use stepwise heating to progressively higher temperatures (followed by cooling in a zero field) to remove less stable portions of the magnetization. Thus, the laboratory thermal demagnetization data consist of room temperature magnetization measurements after heating to a discrete set of temperature steps.

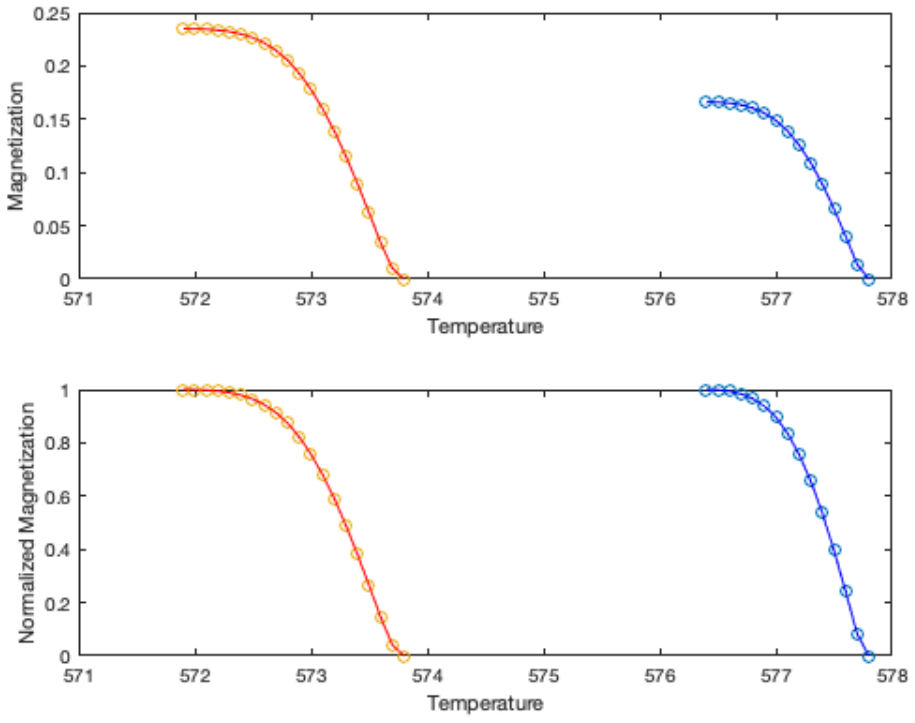

Figure 2.11. a) Example of blocking for assemblage of large (85 nm) elongate magnetite grains during slow cooling (red) and fast cooling (blue). Slow cooling shown reflects 100 kyr duration to cool from 580°C to 500°C. The fast cooling time is selected to match a half hour cooling (about a minute for cooling from 580°C to 500°C) during laboratory treatment. The applied field was 30 μT in each simulation. Note that the magnetization during slow cooling is approximately 41% larger. b) Normalized blocking for the same assemblage shown in (a). The normalized data are used to map blocking temperatures during slow cooling to the corresponding blocking temperatures at laboratory time scales (see text).

An initial step in our modeling involves mapping of the blocking temperature range during slow cooling to the corresponding temperatures at which this remanence will be unblocked during a laboratory thermal demagnetization experiment. Figure 2.11 illustrates this mapping procedure for one population of randomly oriented, elongate magnetite particles 85 nm in size. The magnetization acquired during slow cooling (red curves) occurs at lower temperatures and over a somewhat larger temperature range (onset of blocking at 573.8°C and complete blocking by 571.9°C) than for laboratory cooling (blue curves). The blocked magnetization after slow cooling (100 kyr duration from 580°C to 500°C) is approximately 40% higher, reflecting the closer approach to equilibrium magnetization possible during prolonged cooling (e.g. Nagy et al., 2021; Dodson and McClelland Brown, 1980; Halgedahl et al., 1980).

In order to simulate laboratory thermal demagnetization data, it is necessary to associate the range of blocking temperatures during slow cooling with the corresponding temperature at which the magnetization would be removed (unblocked) by heating over laboratory time scales. As described above, the blocking temperature range obtained from the *sd-cooling* program for each grain size was initially characterized at 101 temperatures. In our model, we track the magnetization at 0.1°C intervals from 580°C (the Curie temperature of magnetite) to 49°C, a temperature cool enough for complete blocking of all grain sizes of interest. The blocked magnetization for both slow and fast cooling is first sampled at 0.1°C intervals (circles in Figure 2.11), typically resulting in a different number of 0.1°C temperature steps for each cooling time. Within MATLAB, we create the arrays of 101 temperatures at 0.1°C intervals within a subroutine named “makeA.m”. It can be used for both slow and fast cooling. The blocked magnetization curves are normalized to 1.0 (complete blocking, Figure 11(b)) and then the

magnetization at each 0.1°C step in the slow-cooling curve is mapped to the closest 0.1°C step in the fast-cooling curve with the same normalized percentage of blocking. This mapping is done in another subroutine named “mapTb.m”, and its information is recorded in a two-dimensional array (Aindex) of temperature indices that can be used to look-up the unblocking temperature at laboratory time scales that corresponds to blocking during slow cooling.

2.4 – Modeling magnetization of a slowly-cooled intrusion

We are now in a position to describe our MATLAB code for modeling the magnetization of a slowly-cooled intrusion. In addition to the blocking temperature information described above (all derived from *sd-cooling*) there are several other parameters that may be specific for each intrusion modeled. These include the distribution of grain sizes (and associated blocking temperatures) in samples from the intrusion, the thermal history of the intrusion that determines the cooling time of a given sample, and finally the variation of the geomagnetic field during cooling. We defer a discussion of specific field models to the Results chapter; the remaining components of the model are described here.

The main routine, "ModelIntrusion.m", is subdivided into a small number of code blocks that implement certain tasks. The first of these code blocks defines several parameters that are related to the data saved from *sd-cooling*. Decreasing temperature (580°C to 49°C) is tracked in 0.1°C steps, sufficient to account for the entire range of grain sizes and blocking temperatures modeled in *sd-cooling*. This temperature dimension (nT = 5311) and the number of grain sizes (nsize = 66) are common dimensions throughout much of what follows. The particular slow-cooling rate arrays (e.g. 100 kyr cooling time) and the corresponding laboratory

cooling time arrays to be used are read in here, and the corresponding two-dimensional arrays are reconstructed for use in the model. These arrays (Aslow, Alab) are each [nT x nsize] and define the fraction of blocking that occurs for each grain size. The final step in this initial code block creates the array Aindex [nT x nsize] that serves as a look-up table for converting blocking temperatures during slow cooling to laboratory time scales.

Figure 2.12 illustrates schematically how these arrays are used to calculate the final magnetization for a single sample from the intrusion. The cooling history for the sample is specified from thermal modeling (we return to this below), and this specific history identifies the time at which each 0.1°C interval is encountered. At each of these temperature steps, we then determine what grain sizes have blocking occurring (this is the information stored in the Aslow array) and we use the corresponding time to identify the time-varying geomagnetic field (Bx(t), By(t), Bz(t)) at that time. The resulting incremental magnetizations are recorded in arrays representing the slow-cooling magnetization (SMx, SMy, SMz for the three magnetization components). Multiplying one of these arrays by the corresponding grain size fraction array for the sample then yields the final magnetization acquired during each 0.1°C temperature interval during slow cooling. The acquired magnetization is stored in three one-dimensional arrays of length nT. For comparison with demagnetization data obtained from faster-cooling experiments in the lab, the slow-cooling magnetization array (e.g. SMx) is mapped into the corresponding array for fast cooling (Mx) using the look-up information in array Aindex. From there, the corresponding final magnetization for fast, lab cooling times is formed in the same fashion as for slow cooling.

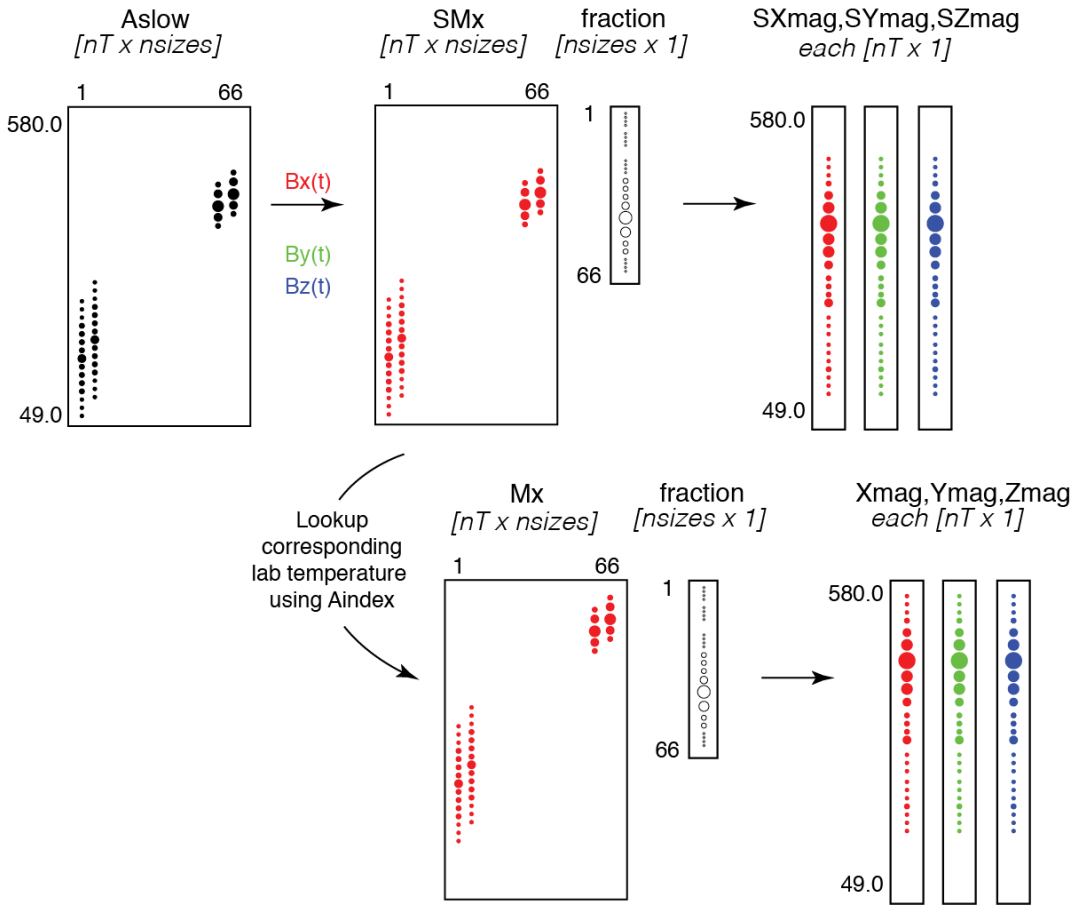

Figure 2.12. Schematic illustrating the calculation of the magnetization acquired during slow cooling (top) and as observed during demagnetization over laboratory time scales (bottom). Matrix Aslow contains the cooled magnetization fraction for each grain size as determined from *sd-cooling*. Symbol size indicates the fraction of the magnetization acquired. The cooling history for the sample is used to determine the corresponding field variation as a function of time (Bx(t), By(t), Bz(t)) for each 0.1°C temperature step. Matrix SMx represents the acquired magnetization for each grain size and temperature step during slow cooling. The corresponding matrix Aindex allows mapping of these slow cooling temperatures to the corresponding (higher) temperatures that would be observed during demagnetization over laboratory time scales (matrix Mx). When multiplied by the grain size fraction for the sample (symbol size proportional to proportion of each grain size), the slow (SMx, SMy, SMz) and laboratory (Mx, My, Mz) yield the magnetization at each 0.1°C temperature step for either initial slow cooling (SXmag, SYmag, SZmag) or as observed during laboratory demagnetization (Xmag, Ymag, Zmag).

There are, of course, a number of additional details that are required for modeling samples in a specific intrusion. For example, we would like to examine how magnetization changes through the intrusion - samples at different stratigraphic positions will have different cooling histories - and this requires that we specify how temperature changes through the intrusion. Another important attribute is the grain size distribution of the samples in the intrusion,

which will in turn determine the specific temperature and time at which the remanence is acquired. In the next two subsections, we document how these two attributes (grain size, thermal history) are specified. Then we complete our description of the modeling process by describing the model output.

2.4.1 – Specifying the grain size distribution

We use samples from the Dufek intrusion (see Chapter 1) to estimate the grain size distribution for use in our model. As noted above, these samples have high blocking temperatures (typically with most remanence removed between 580°C and 500°C) that are interpreted to reflect the dominance of fine-grained, elongate magnetite grains hosted within other silicate minerals. Many of these samples were given a laboratory thermoremanent magnetization (TRM) that was then thermally demagnetized. Because the TRM for all grain sizes was acquired in the same known laboratory field, this data provides the most robust estimate of the relative proportions of different grain sizes contributing to the remanence. The top left panel in Figure 2.13 illustrates the demagnetization behavior of the laboratory TRM for a representative sample.

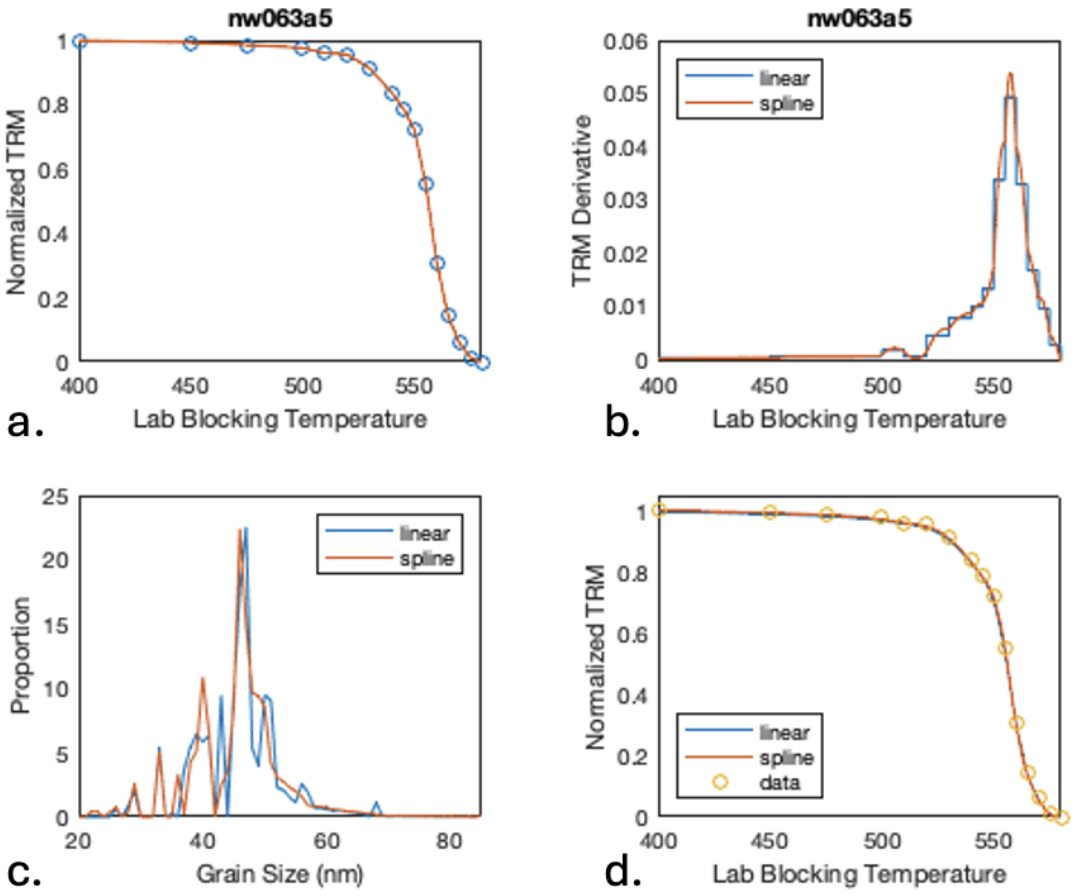

Figure 2.13. Plots illustrating how grain size distribution is estimated for a sample (nw063a5). a) Normalized thermal demagnetization of a laboratory TRM. b) Blocking temperature spectrum = derivative of the curve shown in panel (a). c) Inferred grain size distribution, d) predicted TRM (curves) compared with original TRM demagnetization data from (a). Blue and red curves represent linear and Akima spline fits (see text).

We used some of the built-in functions in MATLAB to estimate the fraction of different grain sizes that would reproduce the TRM demagnetization data. Since the demagnetization occurs over laboratory time scales, the Alab array provides the necessary information to estimate the proportions of various grain sizes. Specifically, each column of Alab [nT x nsize] contains the derivative of the TRM acquired over the temperature range of blocking for a particular grain size. There is one significant difference between these data and the experimentally-determined unblocking of the laboratory TRM: the latter is measured only at a relatively small number of

temperature steps whereas Alab has blocking represented at 0.1°C intervals. So the first step in estimating the grain size distribution is to calculate the derivative of the TRM demagnetization (top left panel, Figure 2.13) at each 0.1°C. We have estimated this in two ways: 1) by linear interpolation between the known temperature steps (leading to the stair step derivative shown in blue in Figure 2.13) and 2) by Akima spline interpolation of these same data (orange curve in Figure 2.13).

This interpolated TRM derivative then constitutes that data vector (d, [nT x 1]) that we wish to fit using linear combinations of the derivative information for each grain size in the Alab array. Because the fractions of each grain size can only be positive, we used the built-in MATLAB routine for non-negative least squares (*lsqnonneg*) to estimate the best fitting grain size distribution. The resulting proportion of each grain size is shown in the bottom left panel and the reconstructed TRM decay (found by integrating the derivatives using MATLAB's *cumtrapz* function) is shown in the bottom right panel. Although there are slight differences in the grain size proportions for the linear and spline interpolations both provide a very good fit to the original TRM demagnetization data. For models using a specific sample grain size distribution we use the solution based on linear interpolation.

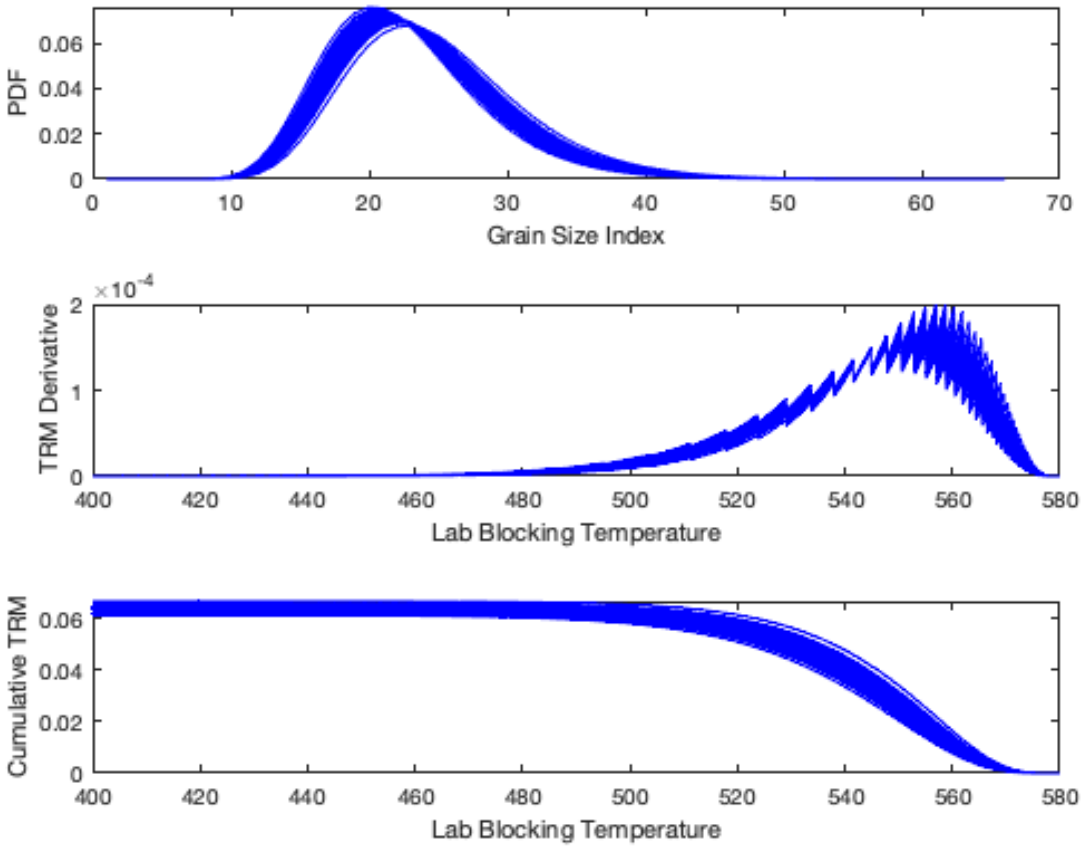

Figure 2.14. Example of representative lognormal grain size distributions (top panel = probability density function) and their associated blocking temperature spectra (middle panel) and normalized remanence decay (bottom panel). A mean grain size index of 23 (± 0.02), correlating to a grain size of 43 nm, was chosen to simulate 101 rocks that are very similar but not identical grain size distributions. The lognormal distribution allows for little variation for a realistic grain size distribution.

While using a particular grain size distribution can be useful for some modeling applications, it is sometimes useful to have a parameterized distribution both to avoid zero magnetization for grain sizes set to zero in the non-negative least squares solution and to simulate some natural variability in grain size distributions across the intrusion. Lognormal distributions have been used previously to model blocking in populations of single-domain particles (e.g. Worm and Jackson, 1988). We have therefore adopted a parameterized lognormal distribution and for this we use the lognormal distribution routines in MATLAB (part of the

Statistics and Machine Learning Toolbox). An example of a lognormal distribution of grain sizes yielding unblocking between about 570° and 500°C is shown in Figure 2.14. The mean of the lognormal distribution is specified in terms of the index of the grain size (here 23, corresponding to a grain size of 43 nm). Variability in the grain size distribution can be simulated by adjusting sigma for the lognormal distribution (sigma = 0.25 shown). This example illustrates how a plausible distribution of TRM unblocking, centered near the 570°-500°C range observed in samples, can be generated using a lognormal distribution.

2.4.2 – Thermal history of modeled samples

Slow cooling of large intrusions is expected to smooth directional and intensity fluctuations of the geomagnetic field. In order to examine the inherent smoothing associated with slow cooling it is useful to model the predicted magnetization of multiple samples distributed throughout the intrusion. To do this, we need an independent estimate of the cooling history of each sample in the intrusion. We use the Heat3D finite element modeling code of Ken Wohletz (see https://www.lanl.gov/orgs/ees/geodynamics/Wohletz/KWare/Index.htm) to quantify the cooling history of a series of samples distributed through an intrusion. Because our MATLAB models are compared to remanence data from the Dufek intrusion (see Chapter 1), we have generated thermal models that estimate the cooling history of this intrusion. The models chosen have also been selected to approximate the cooling times that we chose with the *sd-cooling* code (for additional information on the thermal modeling see Appendix 2).

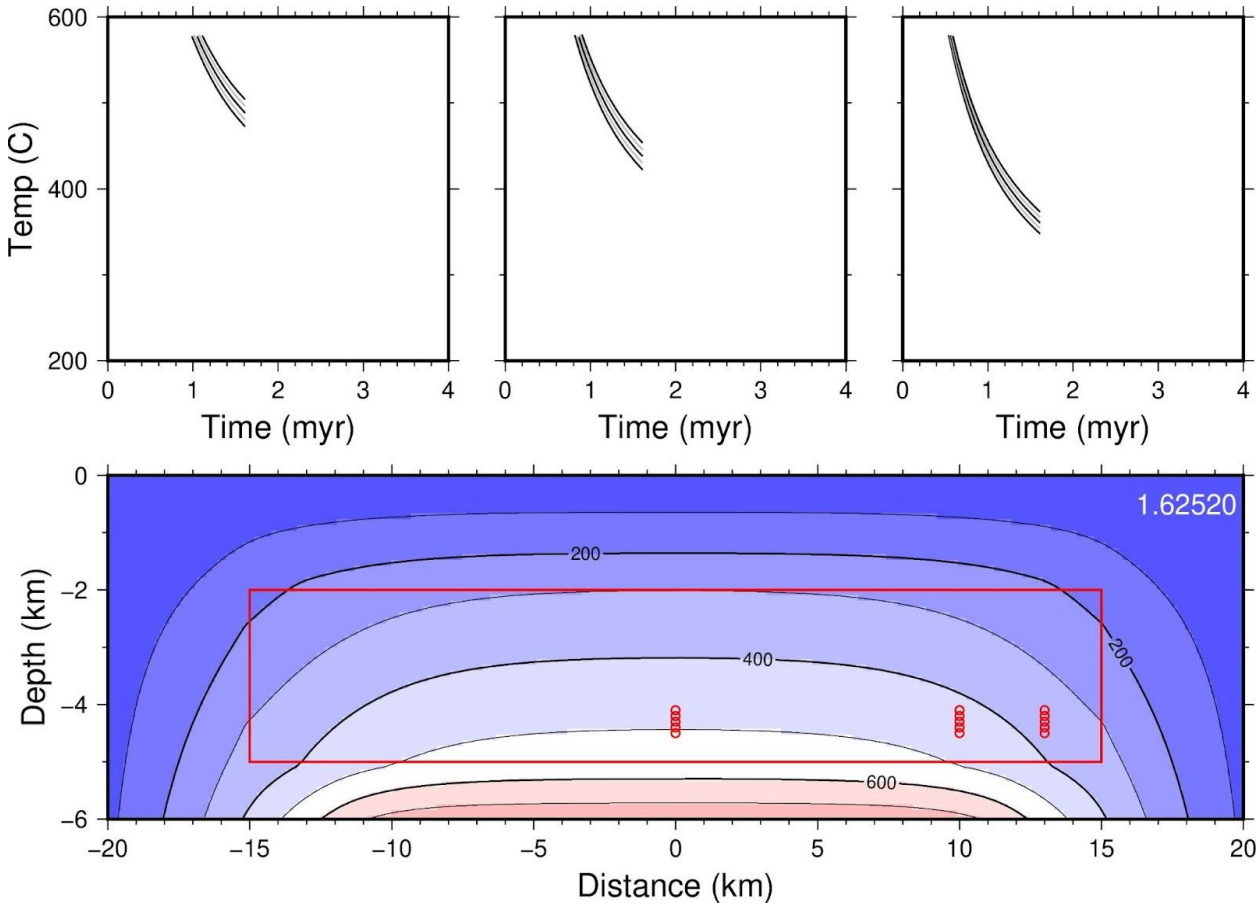

Figure 2.15. Snapshot of Dufek thermal model at 1.62520 million years after emplacement. Bottom panel shows the extent of the intrusion (red lines), temperature contours, and the location of three, 500m sampling profiles through the intrusion (red dots). The evolution of temperature for these sampling locations are shown in the top diagrams.

Figure 2.15 illustrates one such cooling model for the Dufek intrusion (see https://earthref.org/ERDA/2749/); It has a 3 km thick intrusion with its top 2 km below the surface. Although the Dufek intrusion may be part of a larger intrusion (e.g. Ferris et al., 1998), the exposed thickness (~1800 m) in the Dufek range represents a minimum bound on the thickness of the intrusion. Exposures in the Dufek extend for several 10s of kilometers, so we have modeled the intrusion as having a 30 km lateral extent. Our models using the Heat3D software have been calculated assuming an infinite extent of the intrusion in the other horizontal direction; 2.5D models assuming that the intrusion has equal horizontal dimensions would result

in somewhat faster cooling. The modeled temperature evolution is based on a 100 m grid node spacing from which we extract the time-temperature evolution at a series of 6 vertically-distributed nodes representing the cooling for a 500 m stratigraphic section through the intrusion. In our MATLAB code, the temperature variation through time at these 6 nodes (recorded in a so-called "watch.dat" file) is used to interpolate the time-temperature history for a larger set of samples (typically 101) spanning this same 500 m stratigraphic interval. We found that simple linear interpolation of temperatures both in depth and time resulted in some artifacts (streaking of remanence directions on spatial scales that are similar to the spacing of points in the thermal model) in the modeled remanence, so we use a parameterized (parabolic) form to interpolate temperatures at a given time. This enforced the physically realistic parabolic distribution of temperatures at a given time, and linear interpolation of these values in time to generate the final time-temperature paths for each sample to be used in the modeling.

2.4.3 – Model output

Once the parameterized arrays, thermal modeling, and grain size distribution of the Dufek are calculated, we can focus on what gets output from our model. The last section of "ModelIntrusion.m" holds the main loop of the code and is where we loop through each sample while taking into consideration the specifications described above. For example, the fundamental output of the model is all components of the magnetization acquired at 0.1°C temperature steps during the time it was acquired during slow cooling. The equivalent 0.1°C data is also recorded for fast (lab) cooling by mapping the slow cooling magnetization components to the corresponding lab temperature, which will occur at higher temperature. The purpose of having

the corresponding fast cooling time arrays is to compare our model output with thermal demagnetization data measured on samples. These 0.1°C data can be used to produce an animation of the instantaneous magnetization acquired during slow cooling (Appendix 2).

Because we are modeling SD grains, the blocking of remanence during cooling and the unblocking of that remanence during heating (as in a lab demagnetization experiment) occur at the same temperature. We can simulate a laboratory demagnetization experiment by first integrating the 0.1°C magnetization data to give the resultant magnetization at any temperature. For example, the resultant magnetization at the lowest temperature represents the natural remanent magnetization that would be measured without any heating in the lab. Magnetization values for any other temperature in this array represent the remanence that would remain after heating to this temperature. A demagnetization temperature array is made with typical temperature steps chosen for thermal demagnetization experiments. The magnetization remaining after any demagnetization temperature step gets converted into declination, inclination, and intensity data for each demagnetization step, and a "mag.txt" file gets written (Table 2.1) with those values and saved to the working directory. This file contains the simulated data that would be measured during a laboratory demagnetization experiment and is useful for comparing this model to data from the Dufek or any other intrusion.

Table 2.1. The first 5 lines of an example "mag.txt" file

Height (m)	Temperature step (°C)	Circular Standard Deviation	Intensity	Declination	Inclination
-2400	300.0	0.0	0.2817	-179.9	62.4
-2400	350.0	0.0	0.2817	-179.9	62.4
-2400	400.0	0.0	0.2817	-179.9	62.4
-2400	450.0	0.0	0.2815	-179.9	62.4
-2400	475.0	0.0	0.2812	-179.9	62.4

The actual model output is saved in an array named “OneTenth” (Table 2.2) and is representative of the magnetization acquired during slow cooling. A key advantage of our models is the ability to track the time at which the remanence is acquired as temperature falls in 0.1°C increments. In addition to time and temperature, the "OneTenth" output array has the sample depth (for each of 101 modeled samples), declination, inclination and intensity of the magnetization acquired. Because the field variations used for the model include polarity reversals, we found it useful to also include a column with the signed intensity. The sign of this value (- for reverse, + for normal polarity) is used to visually track polarity in animations of the remanence acquisition, as will be discussed in the next chapter.

Table 2.2. The first 5 lines of an example "OneTenth" array as outputted from our model.

Height (m)	Temperature step (°C)	Time (mya)	Declination	Inclination	Unsigned Intensity	Signed Intensity
-2400	531	0.8091	175.0938	61.7886	0.0031	-0.0031
-2400	530.9	0.8092	179.3263	62.8159	0.0032	-0.0032
-2400	530.8	0.8093	-178.2932	62.7120	0.0031	-0.0031
-2400	530.7	0.8095	178.4624	61.4449	0.0028	-0.0028
-2400	530.6	0.8096	176.8936	63.7637	0.0026	-0.0026

Chapter 3 RESULTS

In this chapter, we test the effects of slow cooling on various field models at two different timescales (blocking times of 10 kyr and 100 kyr, corresponding to reference times of 0.54 and 5.4 Ma) to analyze the functionality of our model. We go through a series of simple tests to ensure the correctness of the model. We chose to compare our results with the use of Zijderveld (vector endpoint) plots, which show the cooled remanence (as projections of this vector onto the vertical and horizontal planes) remaining at any temperature. These plots also represent the most typical type of data acquired in a laboratory demagnetization experiment, and are useful since we can predict the output for simple cases such as one in which the same blocking temperature distribution is modeled throughout the intrusion. The vector endpoint diagram portrays the remanence remaining after any laboratory heating (and zero field cooling) step. It's worth noting that these plots show data at progressively higher temperatures, meaning we see the magnetization of the grains with lower blocking temperatures getting removed first.

3.1 – Testing simple field models

The first few tests are simple; We use the "mag.txt" file that has the simulated demagnetization step test to produce Zijderveld plots at two cooling timescales with different simple fields. The first test (shown in Figure 3.1) shows magnetization results acquired over a cooling time of 10 kyr from 580°C to 500°C in a uniform field (i.e. constant intensity and far from any polarity reversal). The remanence was modeled for 101 samples, evenly distributed over 500 m of the intrusion, each with the same lognormal distribution of grain sizes (centered at 43 nm). This grain size distribution has laboratory blocking temperatures between about 570°

and 500°C, with correspondingly lower blocking temperatures (about 400-555°C) during initial slow cooling. The remanence of each individual sample is blocked over about 40 kyr for this relatively slow cooling rate. Because the samples have identical magnetic properties (constant field model and grain size distribution for each sample), we expect that the behavior of the magnetization acquired by each sample would yield identical vector endpoint diagrams during a thermal demagnetization experiment. This is what we see in the modeled demagnetization diagrams (the Zijderveld plots) in the right portion of Figure 3.1. Each sample has an identical initial remanence (after complete cooling) in both direction and intensity. The fraction of the remanence remaining after each temperature step is also identical.

The panels on the left of Figure 3.1 illustrate an important aspect of the modeling, namely that the time at which remanence is acquired varies systematically throughout the intrusion even though the resulting demagnetization diagrams of the fully cooled remanence are identical. The top left panel has a polarity vs time plot with a vertical black bar representing the specific time during cooling that we've chosen to illustrate. The lower left plot below shows the temperature (solid black line) distribution through the intrusion at the same time represented by the vertical black bar in the above plot. For intrusion samples with the same grain size distribution and cooling at the same rate, any given grain size will always acquire its remanence at the same temperature. The only difference, which we see in Figure 3.1, is that remanence gets acquired at different times at different heights throughout the intrusion.

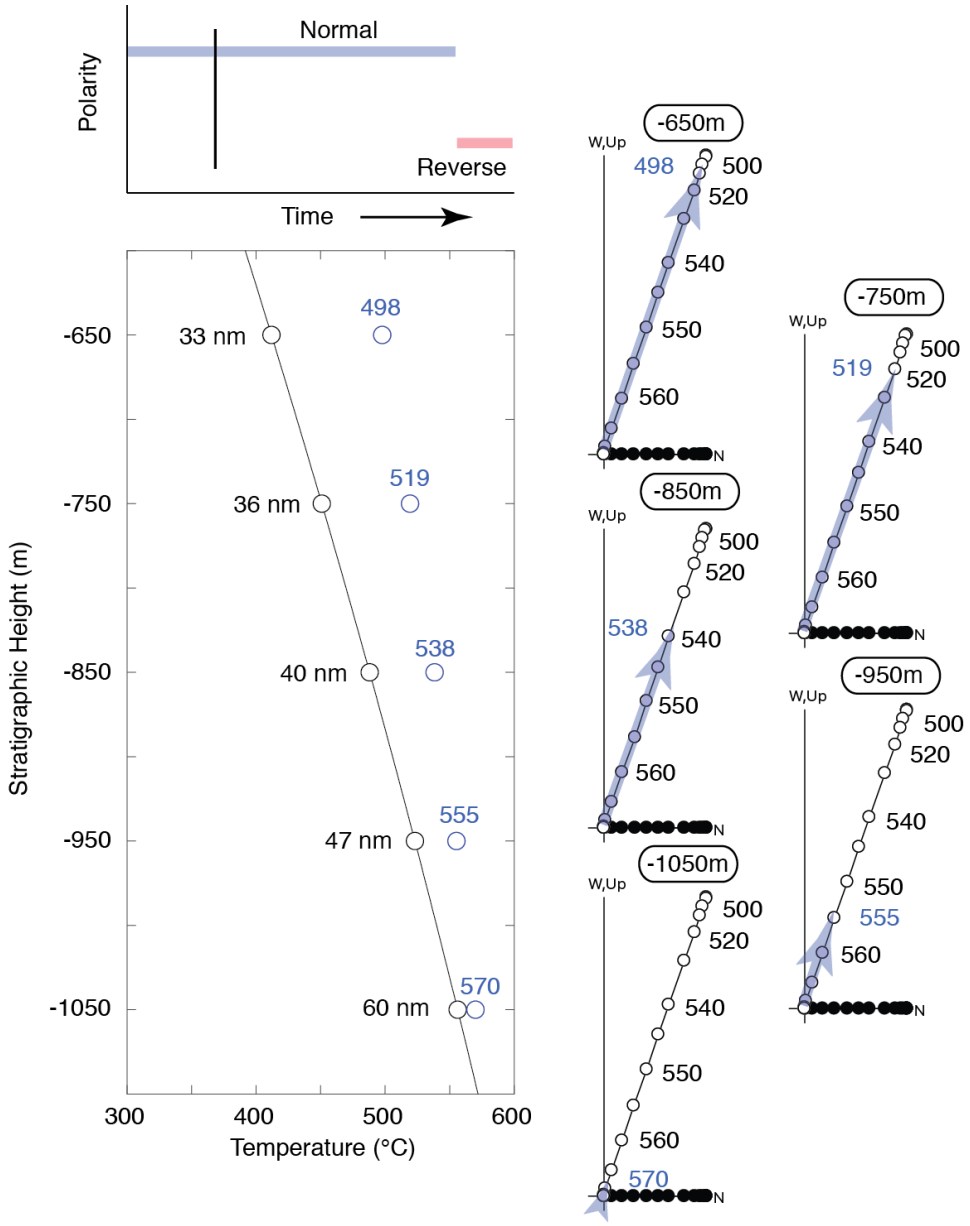

Figure 3.1. Model of a faster cooling time, 10 kyr, with a constant field (normal polarity) and grain size distribution. The time (upper left plot) and temperature (lower left plot) at which the grain sizes (noted to the left of the black points) get magnetized can be related to their corresponding lab temperature (blue points) at which they get demagnetized (shown in the Zijderveld plots). Zijderveld plots consist of two x-y coordinates plotted one on top of the other. One plot has North as the positive x-axis, South as the negative x-axis, West as the positive y-axis, East as the negative y-axis, and has filled circles representing projections on the horizontal plane. The other plot has the same N-S x-axis, but has up as the positive y-axis, down as the negative y-axis, and has open circles representing projections onto the vertical plane. The normal and reverse directions are chosen to have slightly different inclinations for clarity (i.e. to easily see a change in direction). This model is done at a stratigraphic height that is closer to the surface to account for the faster cooling time.

Samples near the top of the intrusion will be at a lower temperature (the top of the intrusion cools faster) and so the remanence being acquired at any instant in time will be carried by smaller grain sizes (with lower blocking temperatures) than for the samples deeper in the intrusion. For example, the uppermost sample modeled (-650 m) is at a temperature of about 410°C (shown by the black circles) and 33 nm grains that have blocking centered on this temperature are being magnetized. The magnetization of this same population of 33 nm grains would be removed at a higher temperature (498°C) over the short time scales of laboratory demagnetization. The bottommost sample (-1050m) is at a temperature of about 560°C, and has a grain size population of 60 nm that has blocking centered at this temperature. The blue arrows on the vector diagrams further highlight the different times at which different portions of the grain size distribution are magnetized during slow cooling or demagnetized during laboratory heating. The topmost sample has experienced the most cooling and remanence for all grain sizes larger than 33 nm will have been blocked by about 410°C (longer blue arrow) whereas the deeper sample at -1050 m will have experienced almost no blocking (shorter blue arrow) at this same time. When demagnetized in the lab, all samples would show identical behavior (i.e. the same remanent direction and intensity at any given demagnetization temperature step) but this masks important information on the time at which the remanence was acquired.

The next test (Figure 3.2) illustrates how a polarity reversal would be recorded in the same intrusion with the same sample characteristics and cooling conditions described above. Here, our expectation is that because the polarity reversal is essentially instantaneous, the cooled remanence should record this polarity transition (as shown by the transition from blue to red arrows in the vector endpoint diagrams) at different temperatures throughout the intrusion sample (i.e. at lower temperatures at shallower depths and progressively higher temperatures

deeper the deeper one gets). Figure 3.2 is a snapshot in time approximately 20 kyr after a simulated reversal as illustrated by the vertical black line within the reverse polarity interval in the top left panel.

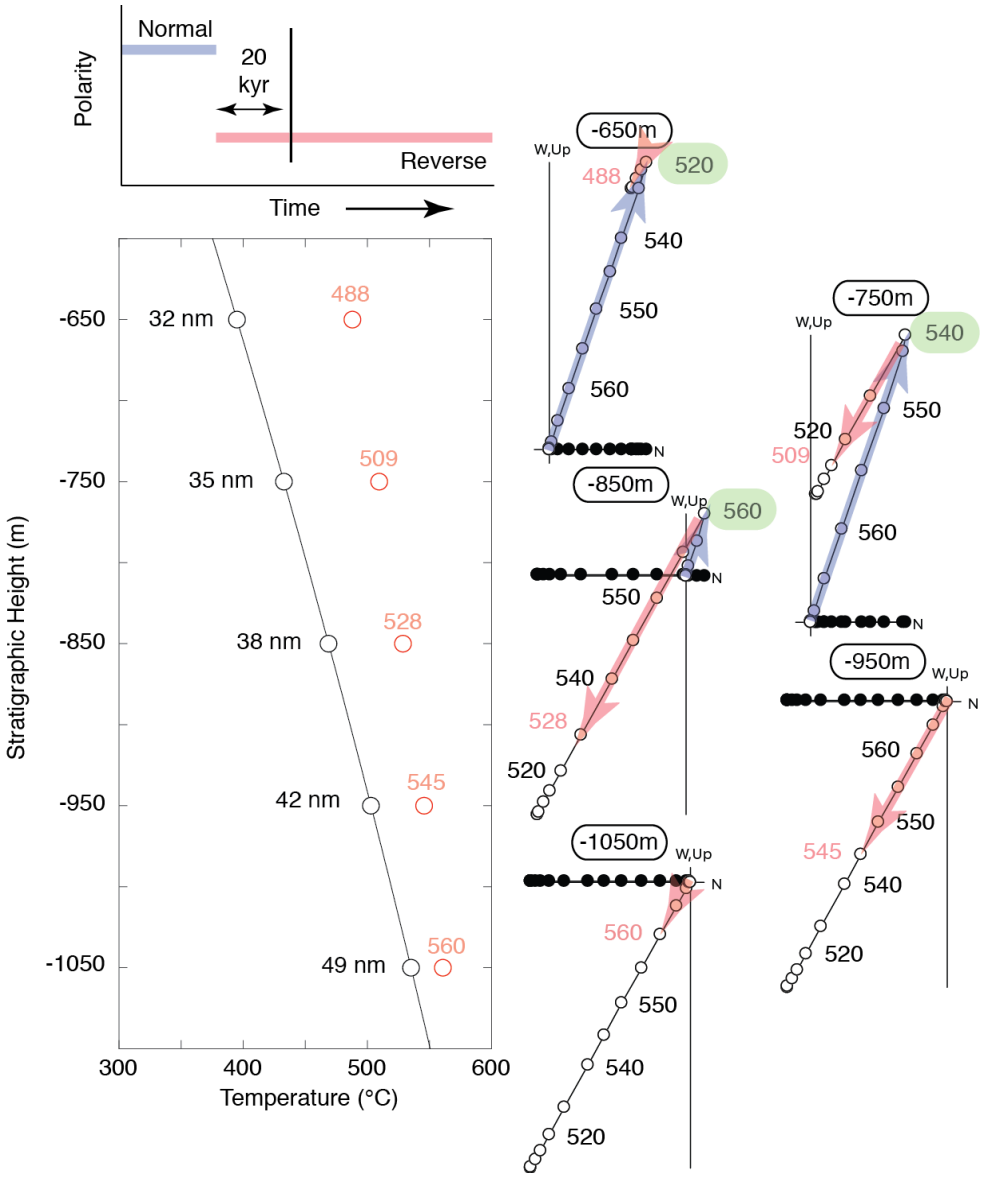

Figure 3.2. Model of a faster cooling time, 10 kyr, with the same parameters as described in Figure 3.1, but with a simulated, instantaneous, polarity reversal. The time (vertical black bar in the upper left panel) is chosen to be 20 kyr after the reversal. The green shaded numbers represent the temperature where the polarity change is recorded in samples, and varies by 40°C over 200 m.

The curve on the height vs temperature plot is still representative of the temperature throughout the intrusion at this point in time, along with the points that show the temperature at which a

population of grains get blocked (black) and the corresponding points at which those same grains get magnetized/demagnetized (red) at lab times.

Because blocking for each sample spans about 40 kyr, the uppermost sample (at about 400°C) is almost completely blocked; the larger grain sizes (with higher blocking temperatures) have already locked in the earlier normal polarity magnetization (blue arrow) and the smaller grain sizes in the sample are recording the current reverse polarity (red arrow). Samples lower in the intrusion (e.g. samples at -950 and -1050 m) were at too high a temperature at the time of the reversal (higher than 580°C) to record the earlier normal polarity field direction and so record only the reverse polarity direction (red arrow). As expected, the temperature at which a polarity transition is recorded in samples (the breakpoint between red and blue arrows, labeled in green in Figure 3.2) does vary systematically with depth in the intrusion. For this cooling time (10 kyr from 580° to 500°C), the model predicts a change in breakpoint temperature of about 40°C over a 200 m stratigraphic interval that should be readily discernible with dense sampling across an intrusion.

We completed the same two tests again, but at 100 kyr instead of 10 kyr cooling time to simulate timescales closer to the Dufek. Figure 3.3 follows the same parameters as above, and depicts a period of constant polarity (constant field model, far from any reversal). One thing to note is that this test is modeled at a section lower in the intrusion to coincide with the slower cooling time. Again, the vector endpoint plots look as we would expect, with all of them being identical, and recording a normal polarity. When comparing them to the ones in Figure 3.1, we see the main difference being that the length of the arrows (laboratory temperature where samples are demagnetized) are not as variable. This reduced variability seen in this slow cooling model correlates to the narrower temperature distribution in the intrusion at its time slice, as it

records less cooling (since it's so slow) than if it were at faster time scales. For example, at the 10 kyr cooling (Figure 3.1), all the samples get blocked over 40 kyr, and a time slice shows a temperature range of ~150°C, whereas the 100 kyr cooling (Figure 3.3), relating to 400 kyr for all samples to get blocked, has a time slice showing a temperature range of only ~50°C.

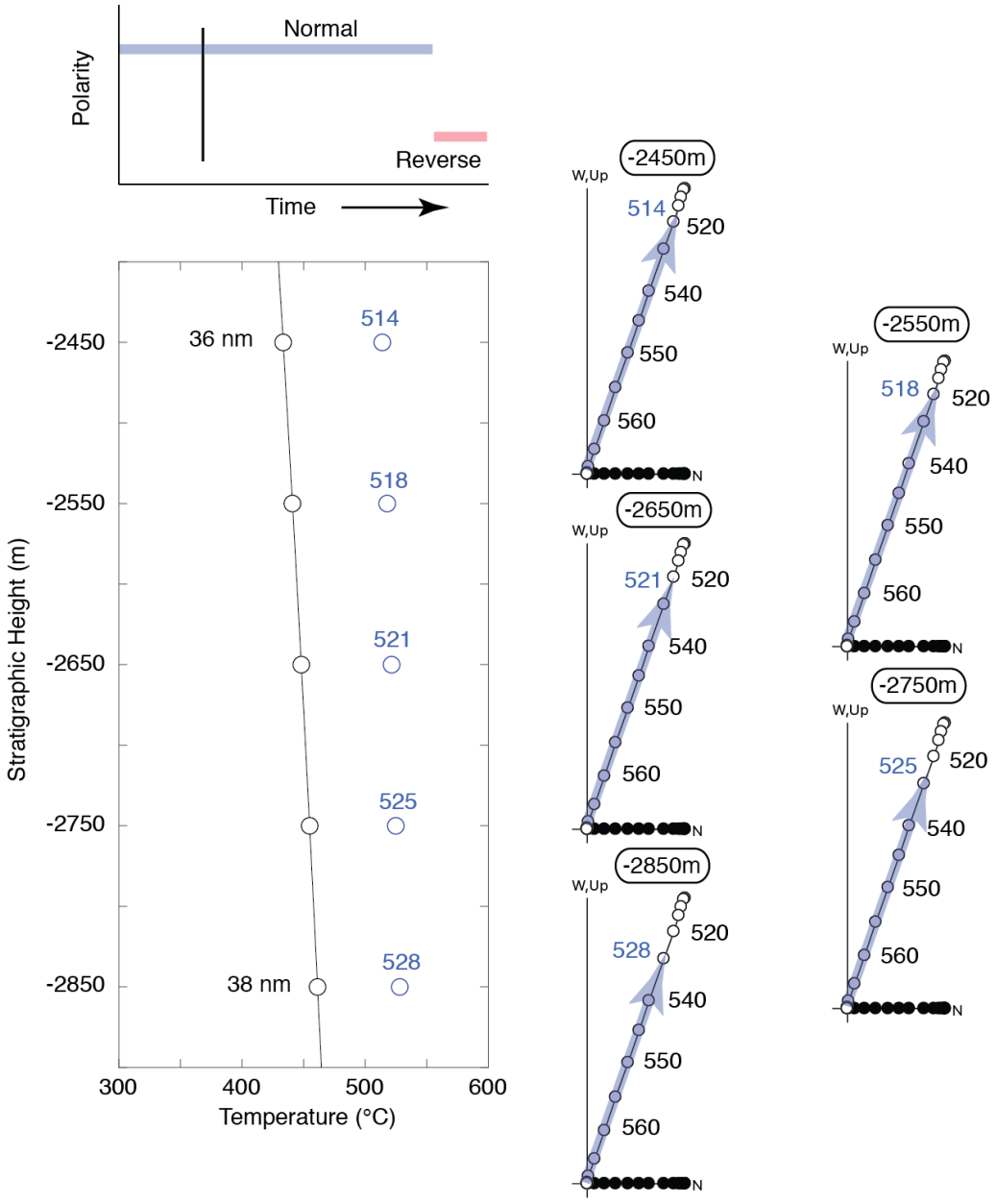

Figure 3.3. Model of a slower cooling time, 100 kyr, with a constant field (normal polarity) and grain size distribution. The time (upper left plot) and temperature (lower left plot) at which the grain sizes (noted to the left of the black points) get magnetized can be related to their corresponding lab temperature (blue points) at which they get demagnetized (shown in the Zijderveld plots). This model is done at a stratigraphic height that is deeper in the stratigraphy to account for the slower cooling time.

The model shown in Figure 3.4 was run with the same type of reversal (normal to reverse polarity) as before, but has the vertical bar representing a point in time 70 kyr after the reversal. Again, we see the time slice capturing a smaller temperature range, but it is still able to show the reversal in the Zijderveld plots.

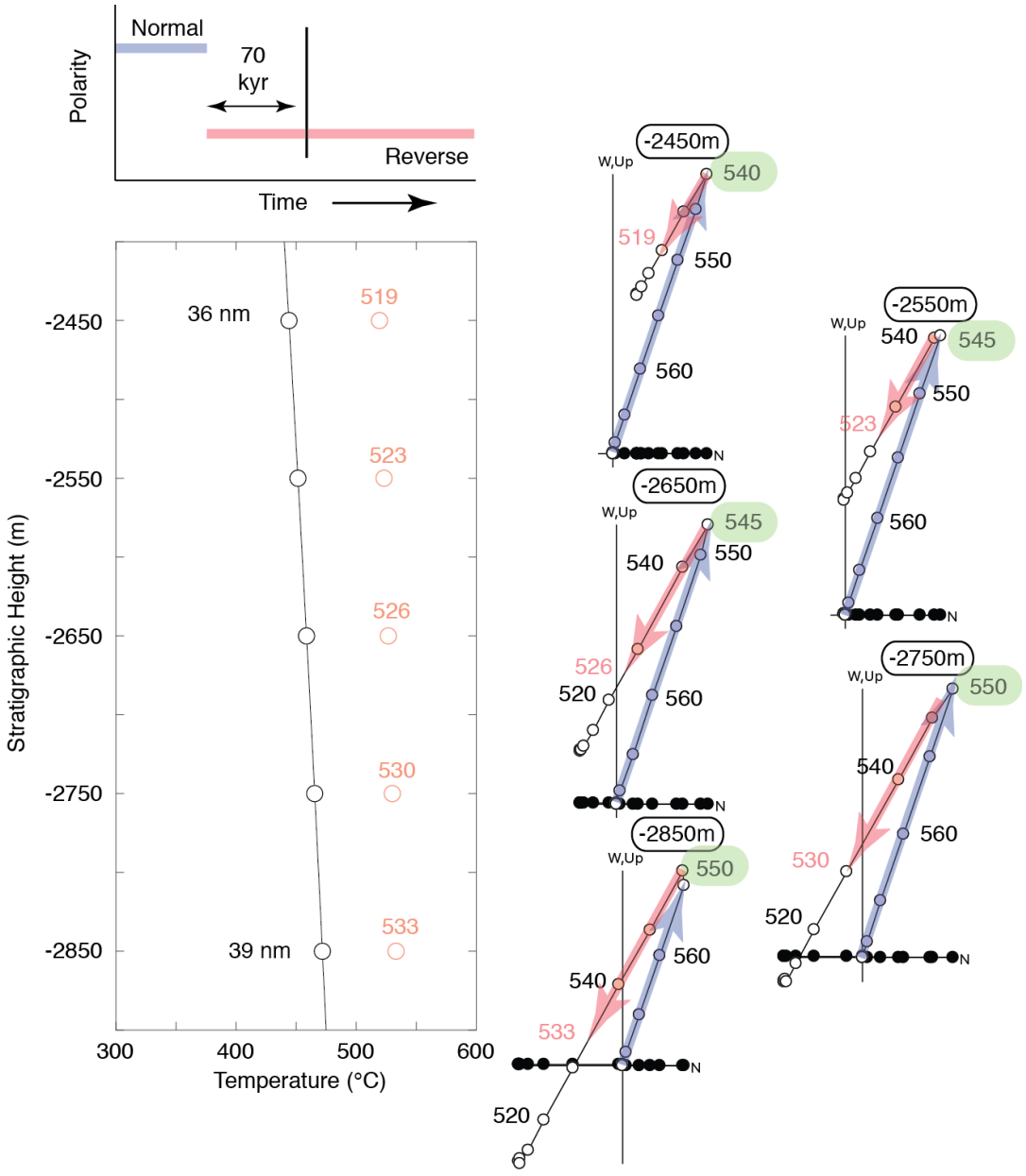

Figure 3.4. Model of a faster cooling time, 10 kyr, with the same parameters as described in Figure 3.1, but with a simulated, instantaneous, polarity reversal. The time (vertical black bar in the upper left panel) is chosen to be 20 kyr after the reversal. The green shaded numbers represent the temperature where the polarity change is recorded in samples, and varies by about 10°C over 500 m.

Similar to Figure 3.2, the top Zijderveld plot shows that the top-most sample captures more of the normal polarity, as it's been cooling for a little longer, and the bottom Zijderveld plot shows that the bottom-most sample has been in the blocking temperature range for less time, and shows more of the reversed polarity magnetization component (red arrows) because of that.

One other key comparison between Figure 3.4 and Figure 3.2 is within the green highlighted numbers, which is the temperature at which the reversal is recorded throughout the stratigraphic section. For the 10 kyr blocking time, we saw a 40°C variation between these temperatures at different depths within the intrusion, and here, for the 100 kyr blocking time, we see only 10°C variation over the 500 m stratigraphic section. The fact that this breakpoint temperature is identical in some samples reflects the relatively coarse (5°C) temperature steps during demagnetization together with the slower cooling. For grains that are blocked near the polarity reversal, the low resultant magnetization over a 5°C interval may reflect the mixture of both normal and reverse polarity.

3.2 – Testing statistical field models

The next few tests were completed with the input of some time varying field models. Initially, we used statistical field models, so-called Giant Gaussian Process (GGP) models, where the non-dipole terms of the field are characterized by Gauss coefficients that are independent samples of a zero-mean Gaussian process (Constable & Parker, 1988). CJ98 is a statistical model produced by Constable & Johnson (1999) that is a modification of the original CP88 Constable & Parker (1988). The CJ98 model is based on directional variation taken from lava samples that

span the last 5 million years and produces a global field model that better reproduces the latitudinal differences in directional and intensity scatter. CJ98 is also used in conjunction with the intensity variations from PADM2M (Ziegler et al., 2011) to produce the first varying field model we test. We combine these two types of models by adding, in varying proportions, the vertical and horizontal components predicted from PADM2M to the component directions from CJ98 (both evaluated at 55°S). Because we were interested in seeing what happens over a reversal (the largest variation of the geomagnetic field), we ran various models incorporating reversals (with ages from the geomagnetic polarity timescale, GPTS 2012, from Gradstein et al., 2012) over the last 2 Ma. Figure 3.5 shows 100 random directions (from the 20,001 total) illustrating the amount of variation we get from the CJ98 field model alone (top panel, a.) and using the combined CJ98 and PADM2M field model (bottom panel, b.) at a 1:1 ratio (meaning we are scaling the mean intensity of PADM2M to match that of CJ98 so both contribute equally). The intrusion sample magnetizations resulting from these field models showed very little directional variability, which is perhaps not surprising given that each field sample is independent, i.e. there is no temporal correlation between field samples.

We also tested whether some degree of temporal smoothing of the directions and intensities in the CG98 statistical model (with or without axial dipole variations from PADM2M) might yield more realistic dispersion in the resulting intrusion magnetization directions. We smoothed the vector components using gaussian filters of various widths. The results shown in Figure 3.5 illustrate representative sections of the filtered field models, using a 4 point (1 sigma) gaussian filter corresponding to a 1 sigma temporal filter of 400 years. As expected, the filtered field model (the red symbols and lines in Figure 3.5) did produce some serial correlation in both

direction and intensity but again the resulting intrusion magnetizations closely paralleled the average field direction.

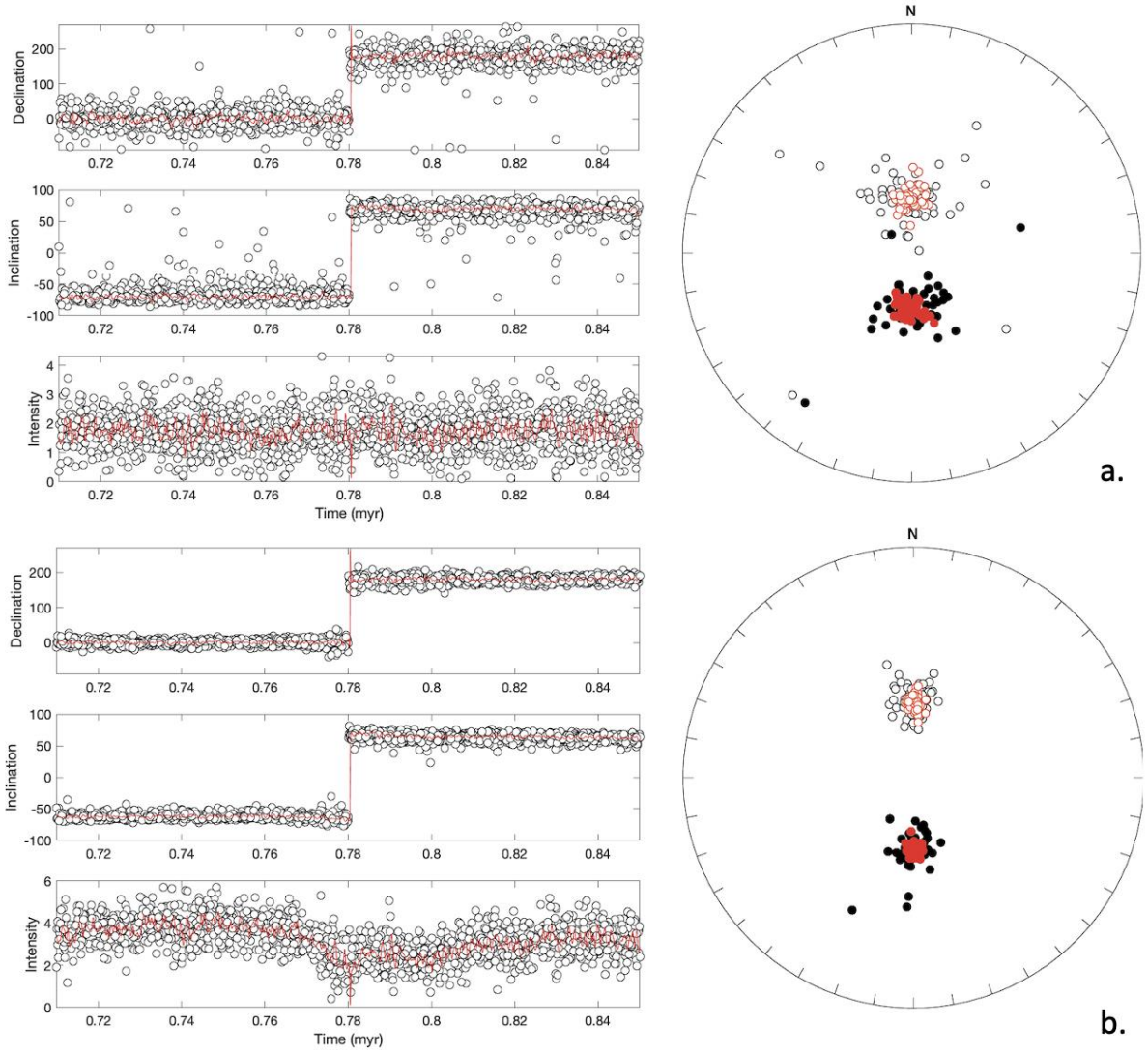

Figure 3.5. Representative field variability at 55°S from the a) the CJ98 statistical field model and b) the CJ98 model combined with axial dipole variations from PADM2M (see text). Panels on the left illustrate representative declination, inclination and intensity variations for about 120 kyr. Polarity reversals were imposed using the dates of reversals in the geomagnetic polarity timescale (GPTS2012, Gradstein et al., 2012). Equal area plots on the right show 100 random directions from the field model. Open circles are upper hemisphere projections and filled circles are lower hemisphere projections. The circles made in black represent the raw data, and the red circles and curves represent the smoothed data.

3.3 – Testing an Earth-realistic field model

Since the statistical models have no correlation between one sample and the preceding or following sample (not serially correlated), we looked elsewhere to find a time varying field that is similar to what we see on Earth. The Geomagnetic Global Field model GGF100k, produced by Panovska et al. (2018), is a spherical harmonic time varying field model derived from sedimentary, archaeomagnetic, and lava flow data spanning the past 100 kyr. As shown in Figure 3.6, GGF100k includes variation that is serially correlated with time, as it is derived from records of Earth's field variations over the past 100 kyr. GGF100k is what we use as our Earth-realistic field model.

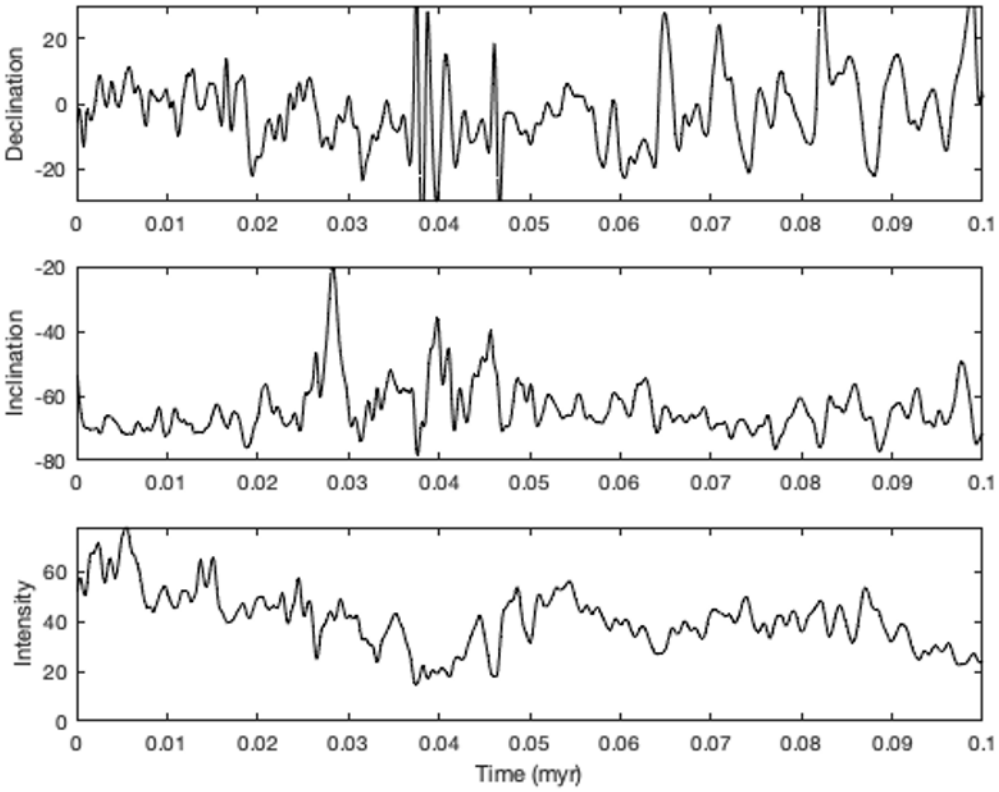

Figure 3.6. Geomagnetic Global Field Model over 100 kyr (GGF100k) evaluated at 60°W, 55°S. From top to bottom, the variation in declination, inclination, and intensity (in T) are shown, and are serially correlated with time. The intensity low and associated directional variations at about 40 kyr reflect the Laschamp excursion. There are no reversals over the last 100 kyr, so we model this excursion event instead.

We tested the GGF100k field model at a faster and a slower cooling time (the same 10 kyr and 100 kyr cooling time as above) to see what types of variation it produced. Since GGF100k only spans 100 kyr, we mirrored it in time to provide a continuous record spanning 0 - 2 Ma, and this is what we use as our input for the time varying field. Figure 3.7 shows a portion of the GGF100k model centered near 0.17 Ma, and Figure 3.8 shows the corresponding intrusion magnetization records at the two different cooling timescales. We choose this timeframe because it shows intensity and inclination variation characteristic of an excursional event. The well-documented Laschamp excursion is a short event near 41 kyr that is associated with low intensity and large directional changes (Panovska et al., 2018). Because our more slowly-cooled model intrusion acquires no remanence over the first ~120 kyr, the Laschamp excursion appears as the intensity low near 0.16 Ma (green shading in Figure 3.7) in the first mirrored copy of the GGF100k field model. The orange shading in both figures represents a time of particularly low inclinations, near 0.17 Ma.

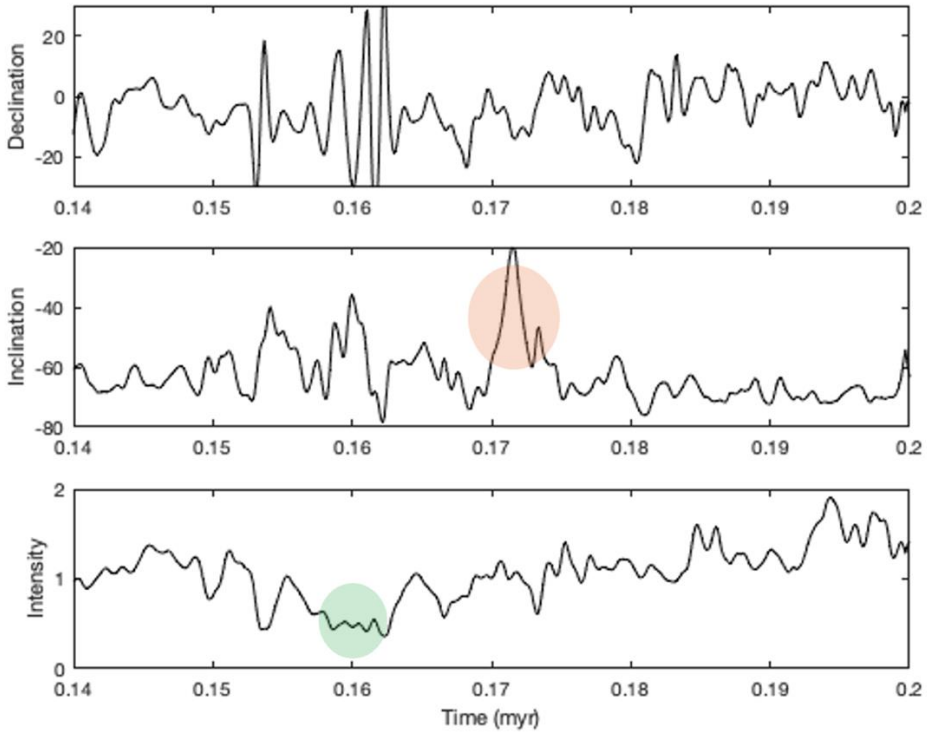

Figure 3.7. Declination, inclination, and intensity variation from GGF100k, centered at 0.17 Ma. The orange shading represents a period of low inclination, and the green shading represents a period of low intensity.

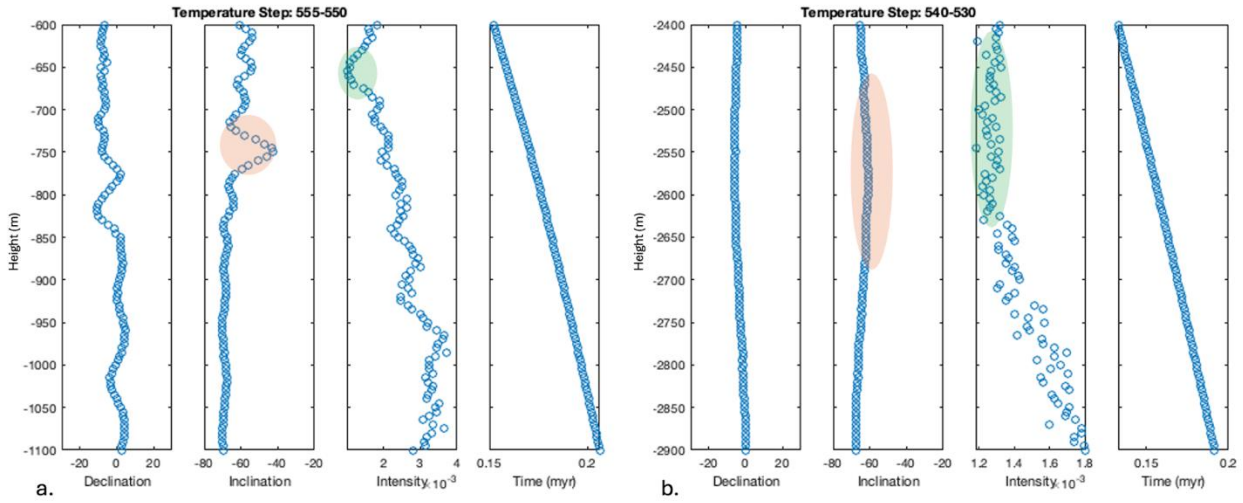

Figure 3.8. Modeled declination, inclination, and intensity data using the GGF100k model for a 500 m stratigraphic section of an intrusion. Panel a) represents a faster blocking time of 10 kyr, is at a shallower depth, and shows temperature steps from 555°C - 550°C. Panel b) represents a slower blocking time of 100 kyr, is at deeper depths, and shows temperature steps from 540°C - 530°C. We highlight these specific temperature steps because they are where we expect to see the excursion event reflected in the components of magnetization. A plot of time is included in both panels to show what age at which the magnetization is acquired. The orange shading corresponds to the inclination low depicted in Figure 3.7, and the green shading corresponds to the intensity low depicted in Figure 3.7. The slower cooling time has more smoothing in the data.

The large and temporally correlated field variations in the GGF100k model allow us to evaluate whether intrusions might record short events such as the Laschamp excursion and how this event might appear at different cooling rates. Declination, inclination, and intensity data were gathered using the temperature steps during lab demagnetization and plotted for a 500 m section of an intrusion. Panel a) in Figure 3.8 is for the 10 kyr cooling time, and it has been offset in time so that the blocking is reasonably well centered to capture the time near 0.16 Ma. Note that this time period is recorded by grains with laboratory blocking temperatures of 555°C to 550°C. Both the intensity low (green shading) and inclination minimum (orange shading) are apparent, though these features are noticeably smoother than in the GGF100k field model. As a reminder, the overall time for blocking is determined by the model lognormal grain size distribution, which is the same for both models, and blocking for a single sample spans 40 kyr for the shorter timescale and 400 kyr for the longer timescale.

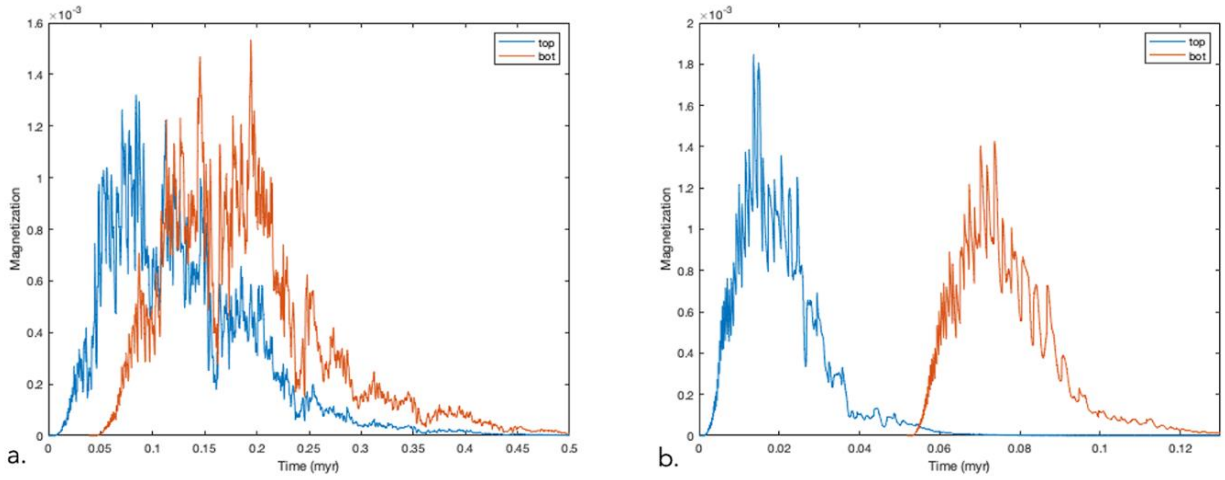

Figure 3.9. Plots showing the time at which grain size distributions acquire their magnetization at the top-most sample and the bottom-most sample. Panel a) is representative of the faster cooling time, 10 kyr, and panel b) is representative of the slower cooling time, 100 kyr.

Figure 3.9 shows that the time, and therefore the temperature, at which the grain size distribution gets magnetized at the top-most sample and the bottom-most sample is different for

the slow cooling and faster cooling. For the 10 kyr cooling time (panel a), Figure 3.9), we see the grain size distributions overlapping more in time.

Panel b) in Figure 3.8 is for the 100 kyr cooling time, and is at a lower temperature step (540°C to 530°C) to capture the same time range. One of the drawbacks of demagnetization data from natural samples is that we don't know the time at which the remanence was acquired, but through the use of our model, we do get information about when things get blocked. Both panels in Figure 3.8 have a time plot on their right that demonstrates the time at which the magnetization was acquired, and the section spans about 50 kyr. You can see the top section gets magnetized earlier in time, correlating to the top samples cooling to the blocking temperature range faster than the bottom. The difference in blocking time will be smaller at faster cooling times, and larger at slower cooling times. Figure 3.9 emphasizes this point, as panel b) shows a broader time range between when the grain size distributions acquire their magnetization at the top-most sample and the bottom-most sample.

One thing to note from Figure 3.8 is that the orange and green shading (corresponding to the inclination and intensity low) look different between the slow and faster cooling times. Because the 100 kyr cooling time has blocking occurring over a much longer time, the declination, inclination, and intensity variations are much smoother. What's imparting the smoothing is that, with slower cooling, any given grain size will be in its narrow blocking temperature range over a longer time period. With that being said, there are still some features that could be recognizable between the original GGF100k field model and the record preserved in intrusions at slow and faster cooling rates. For example, the intensity low (green) in the faster model is at about -650 m, and the increase in intensity as one moves down in the stratigraphy reflects the broad increase in the GGF100k from 0.16 Ma to 0.1 Ma. A similar intensity variation

can be seen in the slower cooled model, but includes more smoothing. The low inclination in GGF100k (orange) also seems to show up in the 10 kyr cooling model at around -750 m, and is consistent with a much smaller, broader inclination change in the 100 kyr model.

Our results are best shown in animations produced using the array "OneTenth". As described above, this array contains the desired declination, inclination, and intensity data at 0.1°C temperature steps, but also includes the depth at which these data are simulated and the time they were acquired. This is one of the first models, if not the first model, that provides both the acquired remanence magnetization during cooling, and the time information along with it. Since we cannot display animations within the text, Figure 3.10 represents a snapshot of our final animation produced using the GGF100k model. This figure tells us a big result: our code works with an Earth-realistic model. We are able to model the acquired remanence for an intrusion with a specific cooling regime with the input of a specific, Earth-realistic field model.

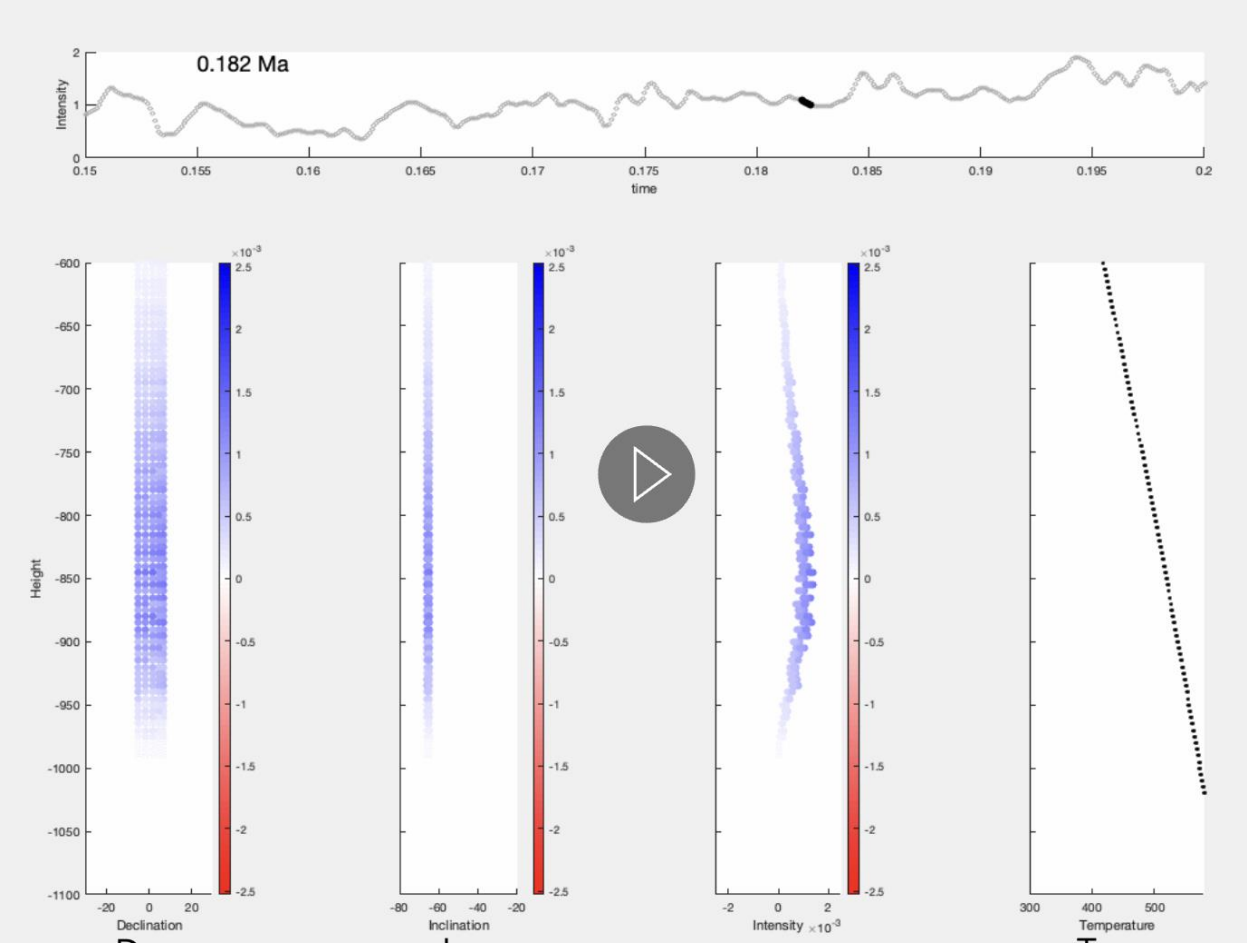

Figure 3.10. Snapshot of an animation of a 500 m stratigraphic section using the GGF100k field model. Intensity vs time plot on the top represents intensity variation throughout time. The bottom plots are representative of a 500 m stratigraphic section, and show declination, inclination, intensity, and the respective temperature at which the magnetization gets acquired at that time step throughout the intrusion. The color bar corresponds to the magnitude of intensity, with blue being positive (normal polarity) values, and red indicating negative (reverse polarity) values. Here we model intensity that varies in the positive realm, so all the points are blue. This animation is available at https://earthref.org/ERDA/2750/.

Figure 3.10 has the declination, inclination, and intensity data for a 500 m stratigraphic section of an intrusion as it varies with the GGF100k intensity for a time from 0.15 to 0.2 Ma (50 kyr). The color of the points correspond to the magnitude of intensity (blue points in Figure 3.10 represent normal polarity, red would be reversed). Variations in the GGF100k field model are evident as lateral shifts in the declination, inclination, and intensity plots, and follow the intensity changes in the above time plot. The height vs intensity plot reflects the concentrated blocking

temperature range in our modeled samples as cooling progresses downward through the intrusion (refer to Figure 3.9). The stratigraphic section will be at progressively higher temperatures as you step deeper through it, and we see the "bulge" of grain size distributions acquiring their magnetization first once the section hits the 580°C - 500°C blocking temperature range. The height vs temperature plot on the right hand side of Figure 3.10 is consistent with the samples getting blocked on the corresponding left graphs. We see the samples acquiring magnetization once that portion of the stratigraphy has reached the starting blocking temperature of 580°C. Notice that the lower most samples have not shown up on the snapshot yet. This is because the temperatures have not gotten within the blocking temperature range yet (they are still at temperatures above 580°C) so they are still too hot to get magnetized. This animation depicts how we can characterize Earth-realistic field variation using intrusions, as described below.

3.4 – Implications for intrusion data

Our results demonstrate that we are able to model geomagnetic field variation at various slow cooling times for large igneous intrusions. Slowly-cooled intrusions have rarely been used to study geomagnetic field variability, as the timing constraints and the effects of the cooling regime on the resulting magnetization are poorly understood. The visualization of the modeled excursion event in Chapter 3.3 (Figure 3.7 & Figure 3.8) gives us hope that we can quantify the amount of smoothing in intrusions accompanying both relatively fast and slow cooling. Our numerical model, in conjunction with Earth-realistic field models, can give a good representation of the geomagnetic variability recorded during slow cooling. If we can understand the smoothing process of acquired remanence over slow cooling from our model, we can apply that to real

intrusion data to potentially characterize the geomagnetic signal recovered from large intrusions. As mentioned in Chapter 1, the magnetic field is a manifestation of the dynamics of our inner Earth. Therefore, having a model that can help provide useful and quantifiable information about geomagnetic field variation in intrusions (which span Earth's age) will allow us to understand the evolution of our planet's deep structure through its lifetime.

APPENDIX

1 – Example directory files

Here we give example files used to run Nagy et al.'s (2021) code, *sd-cooling*, on the University of Liverpool SLURM processing system. Supplemental Figure 1 shows an extended version of the json file given in Chapter 2.1. The outputs of the *sd-cooling* are model, sizes, elongations, directions, and cooling_regime. Each output is given a name within the json file and exported as csv files.


```
{
  "material": "magnetite",

  "sizes": {
    "list": [{"value": 85, "fraction": 1.0}],
    "unit": "nm"
  },

  "elongations": {
    "list": [{"value": 300, "fraction": 1.0}]
  },

  "directions": {
    "distribution": {
      "type": "fibonacci",
      "nbins": 100
    }
  },

  "applied_field": {
    "strength": 30,
    "direction": [1,1,1],
    "unit": "uT"
  },

  "cooling_regime": {
    "ambient_temperature": 15.00,
    "initial_temperature": 579.999,
    "reference_time": 1.7E14,
    "temperature_at_reference_time": 15.15,
    "allowable_percentage_drop": 0.01,
    "stopping_temperature": 50
  },

  "outputs": {
    "model": "/exports/geos.ed.ac.uk/micro_magnetism/MicroMag/Veronica/100k_rerun/rerun056_100k/rerun056_100k_cooling.csv",
    "sizes": "/exports/geos.ed.ac.uk/micro_magnetism/MicroMag/Veronica/100k_rerun/rerun056_100k/rerun056_100k_sizes.csv",
    "elongations": "/exports/geos.ed.ac.uk/micro_magnetism/MicroMag/Veronica/100k_rerun/rerun056_100k/rerun056_100k_elongs.csv",
    "directions": "/exports/geos.ed.ac.uk/micro_magnetism/MicroMag/Veronica/100k_rerun/rerun056_100k/rerun056_100k_direction.csv",
    "cooling_regime": "/exports/geos.ed.ac.uk/micro_magnetism/MicroMag/Veronica/100k_rerun/rerun056_100k/rerun056_100k_cooling_regime.csv"
  },

  "tau0": 1E-10,
  "epsilon": 1E-15,
  "n_polish": 0

}
```


Supplemental Figure 1. Extended json file example that was used to model the remanence acquisition for the largest grain size, 85 nm, at a reference time of 5.4 Ma, or more familiarly a blocking time of 100 kyr for cooling from 580° to 500°C.

Supplemental Figure 2 is a file we needed to use to define where the jobs get submitted within the SLURM processor, and where they end up once they finish running. We also

instituted a statement to send us an email when the code began to run, when it was done, and if it ever failed. That way, we didn't need to have a constant ssh connection to the University of Liverpool's database.

```
#!/bin/bash

#SBATCH --job-name=rerun056_100k

#SBATCH -N 1 # No. of nodes
#SBATCH -n 1 # No. of tasks
#SBATCH -c 1 # No. of cores per task

#SBATCH --time=99:99:99
#SBATCH --chdir=/exports/geos.ed.ac.uk/micro_magnetism/MicroMag/Veronica/100k_rerun/
#SBATCH --mail-user=vyonce@ucsd.edu
#SBATCH --mail-type=BEGIN
#SBATCH --mail-type=END
#SBATCH --mail-type=FAIL

# Load modules
export MODULEPATH=/exports/geos.ed.ac.uk/micro_magnetism/MicroMag/modules:$MODULEPATH
module load boost/1.75.0

# Run model
srun -N 1 /exports/geos.ed.ac.uk/micro_magnetism/MicroMag/Veronica/sd-cooling/build/src_cmdline/cooling/cooling /exports/
geos.ed.ac.uk/micro_magnetism/MicroMag/Veronica/100k_rerun/rerun056_100k/rerun056_100k.json --real-run
```

Supplemental Figure 2. Script used to distinguish where the *sd-cooling* code is run, and where the output files are stored.

Now, you may be wondering how we had the patience to set up each script for each grain size at every timescale. In reality, we created a json template file (Supplemental Figure 3), and looped through each grain size at every timescale using another script (Supplemental Figure 4) that set up all the directories with the filled in json files containing the correct parameters. Then, to submit everything, we used another script (Supplemental Figure 5) that was able to submit multiple runs at once to the queue.

```
{
  "material": "magnetite",

  "sizes": {
    "list": [{"value": 30, "fraction": 1.0}],
    "unit": "nm"
  },

  "elongations": {
    "list": [{"value": 300, "fraction": 1.0}]
  },

  "directions": {
    "distribution": {
      "type": "fibonacci",
      "nbins": 100
    }
  },

  "applied_field": {
    "strength": 30,
    "direction": [1,1,1],
    "unit": "uT"
  },

  "cooling_regime": {
    "ambient_temperature": 15.00,
    "initial_temperature": 579.999,
    "reference_time": 1.7E14,
    "temperature_at_reference_time": 15.15,
    "allowable_percentage_drop": 0.01,
    "stopping_temperature": 50
  },

  "outputs": {
    "model": "#_cooling.csv",
    "sizes": "#_sizes.csv",
    "elongations": "#_elongs.csv",
    "directions": "#_direction.csv",
    "cooling_regime": "#_cooling_regime.csv"
  },

  "tau0": 1E-10,
  "epsilon": 1E-15,
  "n_polish": 0

}
```

Supplemental Figure 3. Json template file.

.

```
#!/bin/bash

### Set the base path, the working directory where individual run
### directories will be created. Specifying the full path
### will allow this script to be run from any directory
### but it might make sense to keep it in the working directory.

BASEPATH=/exports/geos.ed.ac.uk/micro_magnetism/MicroMag/Veronica/100k_rerun/
#BASEPATH=/Users/jeff/Documents/workspace/projects/Laramie/sd-cooling-1.0.2/json/

### Template json and slurm script files. These must be in
### the same directory as this script. The sed commands below
### refer to specific line numbers in the template files so
### caution should be used in editing the templates.

JSON=template_100k_rerun.json
SLURM=template_100k_rerun.script

### Set up three arrays (must all be same size) with variables that
### we want to replace in the template files.

FILES=("rerun036_100k" "rerun037_100k" "rerun038_100k" "rerun039_100k" "rerun040_100k" "rerun041_100k" "rerun042_100k"
"rerun043_100k" "rerun044_100k" "rerun045_100k" "rerun046_100k" "rerun047_100k" "rerun048_100k" "rerun049_100k" "rerun050_100k"
"rerun051_100k" "rerun052_100k" "rerun053_100k" "rerun054_100k" "rerun055_100k" "rerun056_100k")
SIZES=("65" "66" "67" "68" "69" "70" "71" "72" "73" "74" "75" "76" "77" "78" "79" "80" "81" "82" "83" "84" "85")
#FIELDS=("1,0,0" "0,1,0"  "0,0,1"  "1,1,1"  "1,1,1")
#TIMES=("1.7E12"   "1.7E13"   "1.7E14"   "5.3E3"   "6E3")

for idx in "${!FILES[@]}"; do
  FILE=${FILES[$idx]}
  SIZE=${SIZES[$idx]}
 # FIELD=${FIELDS[$idx]}
 # TIME=${TIMES[$idx]}
  echo $FILE $SIZE #$FIELD $TIME
  mkdir $BASEPATH$FILE
 # sed "29s/2E15/$TIME/" $JSON > tmp1
  sed "5s/30/$SIZE/" $JSON > tmp1
 # sed "22s/1,0,0/$FIELD/" tmp2 > tmp3
 # sed "s|#|$BASEPATH$FILE|" tmp3 > $BASEPATH$FILE/$FILE.json
  sed "s|#|$BASEPATH$FILE/$FILE|" tmp1 > $BASEPATH$FILE/$FILE.json
  sed "3s|@|$FILE|" $SLURM > tmp1
  sed "10s|@|$BASEPATH|" tmp1 > tmp2
  sed "21s|@|$BASEPATH$FILE/$FILE.json|" tmp2 > $BASEPATH$FILE/slurm_$FILE.script
done

rm tmp1
rm tmp2
#rm tmp3
```

Supplemental Figure 4. Script including the run parameters and the loop to create directories.

```
#!/bin/bash

for FILES in "rerun036_100k" "rerun037_100k" "rerun038_100k" "rerun039_100k" "rerun040_100k"
"rerun041_100k" "rerun042_100k" "rerun043_100k" "rerun044_100k" "rerun045_100k" "rerun046_100k"
"rerun047_100k" "rerun048_100k" "rerun049_100k" "rerun050_100k" "rerun051_100k" "rerun052_100k"
"rerun053_100k" "rerun054_100k" "rerun055_100k" "rerun056_100k"

do

chmod +x $FILES/slurm_$FILES.script
sbatch -p develop -A develop $FILES/slurm_$FILES.script

done
```

Supplemental Figure 5. Script that submits all the desired scripts for *sd-cooling*.

2 – Thermal models

Our thermal models were motivated by existing dense paleomagnetic sampling through the Jurassic Dufek intrusion in Antarctica. Approximately 600 samples were taken spanning the lowermost 500 m of the intrusion and another 1500 m is exposed at higher elevation, yielding a minimum thickness of about 2 km for the intrusion. Our goal was to generate thermal models that would provide internally consistent, conductive cooling profiles for a 500 m - thick section of the intrusion with average cooling times (580° to 500°C) similar to the timescales (10 kyr, 100 kyr) modeled using the sd-cooling code (Nagy et al., 2021). We use the Heat3D finite element modeling code of Ken Wohletz (see https://www.lanl.gov/orgs/ees/geodynamics/Wohletz/KWare/Index.htm) to quantify the cooling history of a series of samples distributed through an intrusion.

A typical model setup in Heat3D is shown below. All models used a 100 m node spacing, with an overall horizontal dimension of 40 km and a vertical dimension of 6 km. The intrusion shown is 3 km thick, with its top at 2 km and its base at 5 km below the surface and with a horizontal extent of 30 km, similar to the along-strike length of exposures in the Dufek. We used default values in the Heat3D program for a mafic intrusion: liquidus temperature 1250°C, thermal conductivity 1.8 W/mK, specific heat 1200 J/kgK, density 2900 kg/m^3. The country rock was also defined by default values (thermal conductivity 1.0 W/mK, density 2000 kg/m^3) that are broadly consistent with the Paleozoic sediments into which the Dufek intrusion was emplaced. The surface temperature was set to 20°C and the background geothermal gradient was 20°C/km. All models generated assumed a two-dimensional intrusion; three-dimensional models would result in faster cooling.

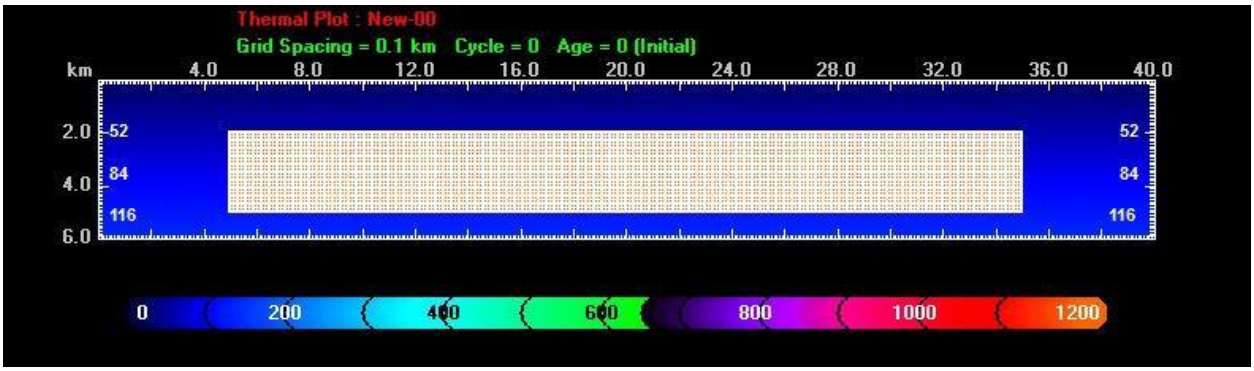

Supplemental Figure 6. A model setup of Heat3D.

Using the parameters above (with instantaneous emplacement of intrusion at t = 0) the intrusion solidifies entirely by 270 kyr. The snapshot below is from movie.avi (see https://earthref.org/ERDA/2749/). This movie tracks the temperature distribution and the temperatures through 500 m portions of the intrusion (red dots). The upper panels show the distribution of temperatures for the three locations at the center of the intrusion as well as 5 km and 2 km from the edge of the intrusion. We extracted cooling histories for a 500 m thick section of the thermal models for use in our MATLAB-based code to model remanence acquisition.

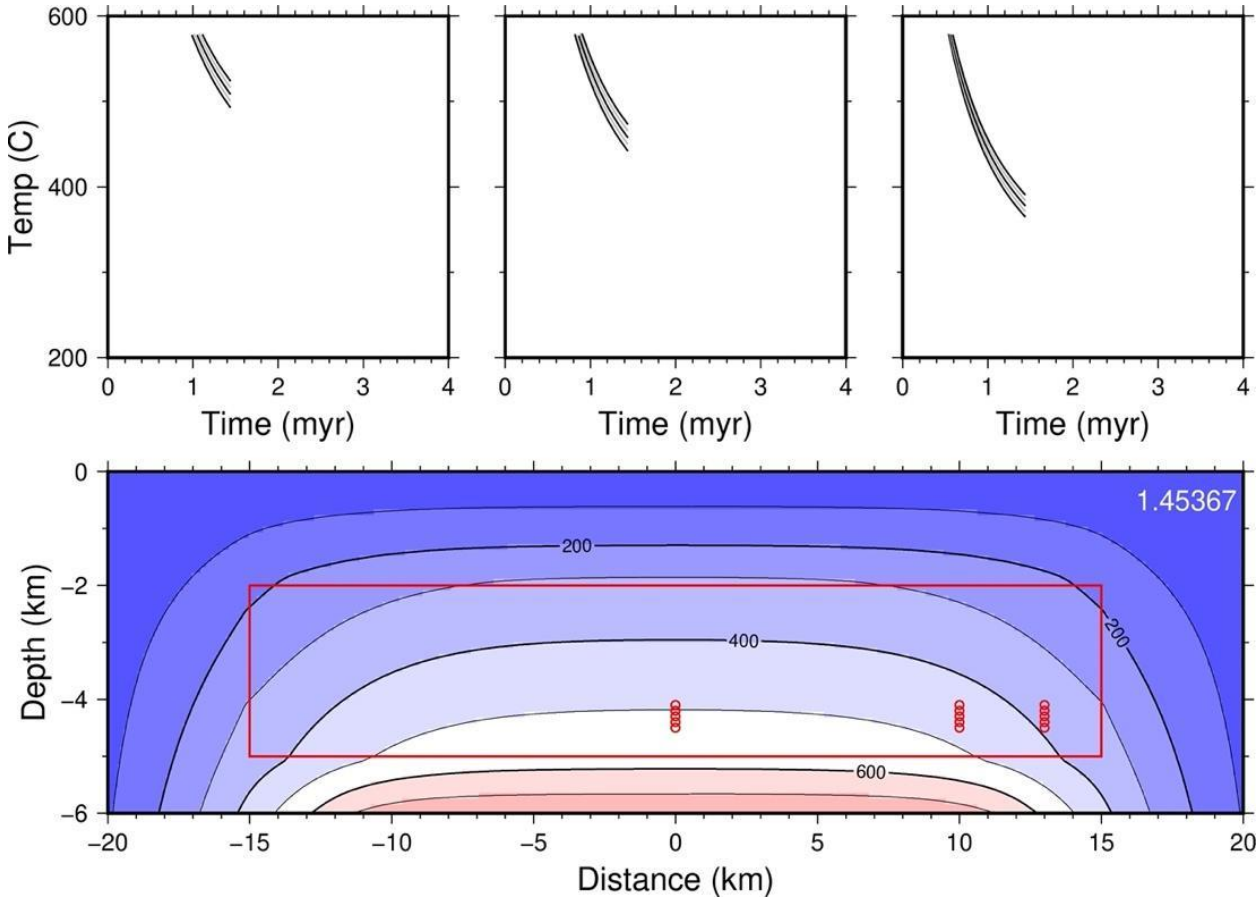

Supplemental Figure 7. Snapshot of a thermal model for the Dufek.

Our modeling of remanence acquisition focused on cooling at two time scales, 20 kyr and 100 kyr, for cooling between 580°C and 500°C that represents the dominant blocking temperature range in samples from the Dufek. To approximate these cooling time scales it was necessary to model a somewhat thinner intrusion (2 km thick) and at variable depths beneath the surface. Our 20 kyr model (20kyr_watch.dat) reflects temperatures in the center of the intrusion and at depths of 600 m to 1100 m below the surface. These depths are near the top of the intrusion, which extends from 500 m to 2500 m depth. Our 100 kyr model (100kyr_watch.dat) reflects temperatures at the center of the intrusion at depths of 2500 m to 3000 m below the surface. These depths are near the vertical center of the modeled intrusion, which extends from 2000 m to 4000 m below the surface.

REFERENCES

Ageeva, O., Bian, G., Habler, G., Pertsev, A. and R. Abart, 2020, Crystallographic and shape orientations of magnetite micro-inclusions in plagioclase, Contrib. Mineral. Petrol., 175:95. https://doi.org/10.1007/s00410-020-01735-8

Beck, M.E., Palaeomagnetism and Magnetic Polarity Zones in the Jurassic Dufek Intrusion, Pensacola Mountains, Antarctica, Geophysical Journal International, Volume 28, Issue 1, May 1972, Pages 49–63, https://doi.org/10.1111/j.1365-246X.1972.tb06110.x

Behrendt, J.C., Drewry, D.J., and Jankowski, E., and England, A.W., 1979, Revision of known area of Dufek intrusion: Antarctic Journal of the Unites States, v.14, no.5.

Berndt, T., Muxworthy, A.R., and Paterson, G.A., (2015), Determining the magnetic attempt time $\tau 0$, its temperature dependence, and the grain size distribution from magnetic viscosity measurements, J. Geophys. Res. Solid Earth, 120, 7322–7336, doi:10.1002/2015JB012283.

Biggin, A.J., Steinberger, B., Aubert, J., Suttie, N., Holme, R. and T.H. Torsvik, 2012, Possible links between long-term geomagnetic variations and whole-mantle convection processes, Nature Geoscience, 5 (8), 526-533.

Bloxham, J., Gubbins, D., and Jackson, A. 1989 Geomagnetic secular variationPhilosophical Transactions of the Royal Society of London. Series A, Mathematical and Physical Sciences 329: 415–502 http://doi.org/10.1098/rsta.1989.0087

Bono, R. K., Tarduno, J.A., Nimmo, F. and R.D. Cottrell, 2019, Young inner core inferred from Ediacaran ultra-low geomagnetic field intensity." Nature Geoscience 12(2): 143-+.

Butler, Robert F. Paleomagnetism: Magnetic Domains to Geologic Terranes. Blackwell Science Inc., 1992

Cande, S. C., and D.V. Kent, (1995), Revised calibration of the geomagnetic polarity timescale for the Late Cretaceous and Cenozoic, J. Geophys. Res., 100(B4), 6093–6095, doi:10.1029/94JB03098.

Cawthorn, R. Grant, and Susan J Webb. "Cooling of the Bushveld Complex, South Africa: Implications for Paleomagnetic Reversals." Geology 41, no. 6 (June 2013): 687–90. https://doi.org/10.1130/G34033.1.

Cawthorn, R.G., and Walraven, F., Emplacement and Crystallization Time for the Bushveld Complex, Journal of Petrology, Volume 39, Issue 9, September 1998, Pages 1669–1687, https://doi.org/10.1093/petroj/39.9.1669

Cheadle, M.J. and J.S. Gee, 2017, Quantitative textural insights into the formation of gabbro in mafic intrusions, Elements, 13:409-414. 10.2138/gselements.13.6.409

Clement, B. Dependence of the duration of geomagnetic polarity reversals on site latitude. Nature 428, 637–640 (2004). https://doi.org/10.1038/nature02459

Constable, Catherine G, and Catherine L Johnson. "Anisotropic Paleosecular Variation Models: Implications for Geomagnetic Field Observables." Physics of the Earth and Planetary Interiors 115, no. 1 (August 1999): 35–51. https://doi.org/10.1016/S0031-9201(99)00065-5.

Constable, C. G., and R. L. Parker. "Statistics of the Geomagnetic Secular Variation for the Past 5 m.y." Journal of Geophysical Research: Solid Earth 93, no. B10 (October 10, 1988): 11569–81. https://doi.org/10.1029/JB093iB10p11569.

Constable, Catherine, and Steven Constable. "A Grand Spectrum of the Geomagnetic Field." Physics of the Earth and Planetary Interiors 344 (November 2023): 107090. https://doi.org/10.1016/j.pepi.2023.107090.

Dodson, M.H. and E. McClelland-Brown, 1980, Magnetic blocking temperatures of single-domain grains during slow cooling, J. Geophys. Res., 85: 2625-2637

Dodson, R., Dunn, J. R., Fuller, M., Williams, I., Ito, H., Schmidt, V.A., and Yee-Ming Wu, Palaeomagnetic record of a late Tertiary field reversal, Geophysical Journal International, Volume 53, Issue 2, May 1978, Pages 373–412, https://doi.org/10.1111/j.1365-246X.1978.tb03748.x

Dunn, J. R., M. Fuller, H. Ito, and V. A. Schmidt. "Paleomagnetic Study of a Reversal of the Earth's Magnetic Field." Science 172, no. 3985 (May 21, 1971): 840–45. https://doi.org/10.1126/science.172.3985.840.

Ferris, J., Johnson, A., and Storey, B. "Form and Extent of the Dufek Intrusion, Antarctica, from Newly Compiled Aeromagnetic Data." Earth and Planetary Science Letters 154, no. 1–4 (January 1998): 185–202. https://doi.org/10.1016/S0012-821X(97)00165-9.

Gee, J.S. and D.V. Kent, Source of oceanic magnetic anomalies and the geomagnetic polarity timescale, 2007, Treatise on Geophysics, vol. 5, M. Kono (ed), Elsevier, pp. 455-507

Gradstein, F.M., Ogg, J.G., Schmitz, M.D., Ogg, G.M. The Geologic Time Scale 2012, vol. 1, Elsevier

Halgedahl, S. L., R. Day, and M. Fuller (1980), The effect of cooling rate on the intensity of weak-field TRM in single-domain magnetite, J. Geophys. Res., 85(B7), 3690–3698, doi:10.1029/JB085iB07p03690.

Johnson, C. L., and P. McFadden (2007), Time-Averaged Field and Paleosecular Variation, Geomagnetism, vol. 5, doi:10.1016/B978-044452748-6.00096-1

Kosterov, A.A., and Perrin, M., Paleomagnetism of the Lesotho basalt, southern Africa, Earth and Planetary Science Letters, Volume 139, Issues 1–2, 1996, Pages 63-78, ISSN 0012-821X, https://doi.org/10.1016/0012-821X(96)00005-2.

Larson, R.L. and P. Olson, 1991, Mantle plumes control magnetic reversal frequency. Earth Planet. Sci. Lett., 107, 437-447.

Letts, S., Torsvik, T.H., Webb, S.J., and Ashwal, L.D., Palaeomagnetism of the 2054 Ma Bushveld Complex (South Africa): implications for emplacement and cooling, Geophysical Journal International, Volume 179, Issue 2, November 2009, Pages 850–872, https://doi.org/10.1111/j.1365-246X.2009.04346.x

Love, J. J. "Palaeomagnetic Secular Variation as a Function of Intensity." Edited by D. Gubbins, D. V. Kent, and C. Laj. Philosophical Transactions of the Royal Society of London. Series A: Mathematical, Physical and Engineering Sciences 358, no. 1768 (March 15, 2000): 1191–1223. https://doi.org/10.1098/rsta.2000.0581.

Lowrie, W. and D.V. Kent, 2004, Geomagnetic polarity timescales and reversal frequency regimes, in: Channell, J.E.T., Kent, D.V., Lowrie, W. and Meert, J. (eds). AGU Geophysical Monograph 145: Timescales of the Paleomagnetic Field, pp. 117-129, Washington D.C., American Geophysical Union.

Moulin, M., F. Fluteau, V. Courtillot, J. Marsh, G. Delpech, X. Quidelleur, M. Gérard, and A. E. Jay (2011), An attempt to constrain the age, duration, and eruptive history of the Karoo flood basalt: Naude's Nek section (South Africa), J. Geophys. Res., 116, B07403, doi:10.1029/2011JB008210.

Nagy, Lesleis, Wyn Williams, and Lisa Tauxe. "Estimating the Effect of Cooling Rate on the Acquisition of Magnetic Remanence." Geophysical Research Letters 48, no. 22 (November 28, 2021): e2021GL095284. https://doi.org/10.1029/2021GL095284.

Néel, L., (1949). Théorie du traînage magnétique des ferromagnétiques en grains fins avec application aux terres cuites, Ann. Géophys., 5, 99-136.

Panovska, S., Constable, C. G., & Brown, M. C. (2018). Global and regional assessments of paleosecular variation activity Over the Past 100 ka. Geochemistry, Geophysics, Geosystems, 19, 1559–1580. https://doi.org/10.1029/2017GC007271

Pechersky, D. M., A. A. Lyubushin, and V. S. Zakharov. "Continuous Record of Geomagnetic Field Variations during Cooling of the Monchegorsk, Kivakka and Bushveld Early Proterozoic Layered Intrusions." Russian Journal of Earth Sciences 6, no. 6 (January 12, 2005): 391–456. https://doi.org/10.2205/2004ES000158.

Prévot, M., Derder, M.E., McWilliams, M., and Thompson, J., Intensity of the Earth's magnetic field: Evidence for a Mesozoic dipole low, Earth and Planetary Science Letters, Volume 97, Issues 1–2, 1990, Pages 129-139, ISSN 0012-821X, https://doi.org/10.1016/0012-821X(90)90104-6.

Roberts, M., 2020, How to evenly distribute points on a sphere more effectively than the canonical Fibonacci Lattice. https://extremelearning.com.au/how-to-evenly-distribute-points-on-a-sphere-more-effectively-than-the-canonical-fibonacci-lattice/

Schneider, D. A., and D. V. Kent (1990), The time-averaged paleomagnetic field, Rev. Geophys., 28(1), 71–96, doi:10.1029/RG028i001p00071.

Selkin, P. A., J. S. Gee, W. P. Meurer, and S. R. Hemming. "Paleointensity Record from the 2.7 Ga Stillwater Complex, Montana." Geochemistry, Geophysics, Geosystems 9, no. 12 (December 2008): 2008GC001950. https://doi.org/10.1029/2008GC001950.

Stoner, E.C., and Wohlfarth, E.P., 1948. A mechanism of magnetic hysteresis in heterogeneous alloysPhilosophical Transactions of the Royal Society of London. Series A, Mathematical and Physical Sciences240599–642 http://doi.org/10.1098/rsta.1948.0007

Tauxe, L., Banerjee, S.K., Butler, R.F., & van der Voo, R. (2018) Essentials of Paleomagnetism, 5th Web Edition, La Jolla, CA: University of California Press. https://earthref.org/MagIC/books/Tauxe/Essentials/#x1-140002

Tauxe, L. and H. Staudigel, 2004, Strength of the geomagnetic field in the Cretaceous Normal Superchron: New data from submarine basaltic glass of the Troodos Ophiolite, G3, 5 Q02H06, doi:10.1029/2003GC000635

Tauxe, L., and T. Yamazaki. "Paleointensities." In Treatise on Geophysics, 461–509. Elsevier, 2015. https://doi.org/10.1016/B978-0-444-53802-4.00107-X

Worm, H.-U. and M. Jackson (1988). "Theoretical time-temperature relationships of magnetization for distributions of single domain magnetite grains." Geophys. Res. Lett. 15: 1093-1096.

Ziegler, L. B., C. G. Constable, C. L. Johnson, and L. Tauxe. “PADM2M: A Penalized Maximum Likelihood Model of the 0-2 Ma Palaeomagnetic Axial Dipole Moment: PADM2M Revised.” Geophysical Journal International 184, no. 3 (March 2011): 1069–89. https://doi.org/10.1111/j.1365-246X.2010.04905.x.